Available online at www.sciencedirect.com

ScienceDirect

Geochimica et Cosmochimica Acta 259 (2019) 270–287

Geochimica et Cosmochimica Acta

www.elsevier.com/locate/gca

Perspectives on provenance and alteration of suspended and sedimentary organic matter in the subtropical Pearl River system, South China

Baozhi Lin [a,b], Zhifei Liu [a,*], Timothy I. Eglinton [b,*], Selvaraj Kandasamy [c], Thomas M. Blattmann [b], Negar Haghipour [b,d], Gert J. de Lange [a,e]

[a] State Key Laboratory of Marine Geology, Tongji University, Shanghai 200092, China
[b] Geological Institute, Department of Earth Sciences, ETH Zürich, 8092 Zürich, Switzerland
[c] Department of Geological Oceanography and State Key Laboratory of Marine Environmental Science, Xiamen University, Xiamen 361102, China
[d] Laboratory of Ion Beam Physics, ETH Zürich, Otto-Stern-Weg 5, 8093 Zürich, Switzerland
[e] Department of Earth Science-Geochemistry, Geosciences, Utrecht University, 3584 CD Utrecht, the Netherlands

Received 14 March 2019; accepted in revised form 11 June 2019; available online 20 June 2019

Abstract

Large river systems accumulate, process, and transport huge quantities of organic matter (OM) from their catchments, part of which is exported to the ocean. Although this suite of processes comprises an important component of the global carbon cycle, integrated studies examining the nature and extent of OM processing on a basin-wide scale remain rare. Here, we provide an overview of provenance and composition of OM in suspended and deposited sediments within the Pearl River watershed in South China. We present new data on the organic carbon (OC) and total nitrogen (TN) contents, stable carbon and radiocarbon isotopic compositions of OC ($\delta^{13}C$ and F_m), as well as grain size distribution and mineral-specific surface area of Pearl River sediments. These results are combined with published data on suspended particulate matter (SPM) and soil profiles in the Pearl River watershed in order to determine the provenance and transformation of OM in this large subtropical fluvial system.

We find that the low ^{14}C contents, expressed as fraction modern (F_m) values, in suspended (F_m: 0.58–0.87) and sedimentary OM (F_m: 0.38–0.82) are attributed to contributions from ^{14}C-depleted soils, bedrock, as well as riverine primary productivity (R_{pp}) that utilizes ^{14}C-depleted sources of dissolved inorganic carbon (DIC). For SPM, soil OM (F_m: 0.87 ± 0.13) is inferred to be the dominant fraction during the wet season, whereas the contributions of R_{pp} (F_m: 0.86 ± 0.04) and petrogenic OC (devoid of ^{14}C) are enhanced during the dry season. This manifests itself in differences in OC_{soil}, OC_{Rpp}, and OC_{petro} contributions in SPM between wet and dry seasons (1.05 ± 0.18 vs. $1.20 \pm 0.50\%$, 0.16 ± 0.03 vs. $0.32 \pm 0.15\%$ and 0.21 ± 0.07 vs. $0.38 \pm 0.19\%$). During erosion and transport, the most labile OM in the top soil is rapidly degraded, as indicated by a stronger contribution from soil CO_2 into riverine DIC during the wet season and flood event ($39 \pm 1\%$ and $45 \pm 3\%$) compared to the dry season ($31 \pm 2\%$). River sediments are primarily accumulated during the wet season when suspended sediment fluxes are high. Refractory deep soil OM (F_m: 0.74 ± 0.07) dominate in these sediments, whereas moderately labile soil OM components are further degraded during settling and storage. This sedimentary OM is predominantly composed of aged soil ($92 \pm 4\%$), with a minor contribution from bedrock ($7 \pm 4\%$) and negligible input from R_{pp} ($0.2 \pm 0\%$). The longitudinal changes in the composition of suspended and sedimentary OM are mainly controlled by input of R_{pp} and ongoing degradation processes in the river system. The riverine particulate OC flux to the Pearl River estuary and ocean thus contains a mixture of soil,

* Corresponding authors.
E-mail addresses: lzhifei@tongji.edu.cn (Z. Liu), timothy.eglinton@erdw.ethz.ch (T.I. Eglinton).

https://doi.org/10.1016/j.gca.2019.06.018

petrogenic and R_{pp} OM, all exhibiting relatively low F_m values. The riverine OM transformation and dynamics are important for the short-term carbon cycle, whereas the remaining signature and fate of the extensively processed, refractory OM has implications for the long-term carbon cycle.

Keywords: Organic matter; Carbon isotope; Radiocarbon; Organic matter degradation; Sediment; Pearl River; South China

1. INTRODUCTION

Soils (1950 Pg C, Pg = 10^{15} g) and vegetation (550 Pg C) comprise the two major active organic carbon (OC) pools on the Earth's surface that exchange carbon with the atmosphere on millennial or shorter timescales (Berner, 1989; Hedges and Oades, 1997; Sarmiento and Gruber, 2002). The total amount of OC stored in these two pools is approximately three times the carbon stock in the form of carbon dioxide (CO_2) in the preindustrial atmosphere (730 Pg C; Siegenthaler and Sarmiento, 1993; Sarmiento and Gruber, 2002). The largest OC reservoir on Earth is fossil OC residing in sedimentary rocks (15 million Pg C; Berner, 1989). Although recycling and reburial of fossil OC exert no effect on atmospheric CO_2, oxidation of fossil OC during erosion and riverine transport releases CO_2 from long-term geological storage to the atmosphere (Blair et al., 2003; Galy et al., 2008). River systems provide the primary mechanism for export of OC from land to ocean (Cole et al., 2007; Aufdenkampe et al., 2011), discharging ~0.43 Pg OC annually, of which ~0.20 Pg is in particulate form (Schlünz and Schneider, 2000; Kandasamy and Nagender Nath, 2016). They thus form an important component of the global carbon cycle, with burial of terrestrial OC in ocean sediments contributing to long-term regulation of the Earth's climate (Burdige, 2005; Bauer et al., 2013) and leading to formation of fossil fuels deposits on geologic timescales (Berner, 1982; Hedges et al., 1997; Galy et al., 2008). Changes in surface reservoir carbon inventories (soils, rivers and the ocean) can influence atmospheric CO_2 concentrations (Galy and Eglinton, 2011; Cartapanis et al., 2016), with rivers playing important and dynamic role in carbon cycling on both regional and global scales.

Riverine suspended particulate matter (SPM) and sediment deposits contain OM, exhibiting a range of ages and reactivities by virtue of their different sources, and storage and transport histories (Blair and Aller, 2012; Marwick et al., 2015; Leithold et al., 2016). This includes biospheric OM derived from aquatic primary production and vascular land plants and associated detritus and soils, as well as ancient "petrogenic" OM from bedrock erosion. In steep, weathering-limited small mountainous rivers, the latter may escape oxidation and become a major component of riverine suspended and sedimentary OM (Blair et al., 2003; Hilton et al., 2010). However, in transport-limited large fluvial systems, OM is subject to extensive oxidation and transformation during transit and storage in intermediate reservoirs (Blair et al., 2004; Leithold et al., 2016). Rivers can thus serve as sites of intense OM recycling and degradation (Blair and Aller, 2012), where particulate OM is subject to myriad biological (e.g. microbial utilization), chemical (e.g. photochemical degradation; sorption/desorption) and physical (e.g. sedimentation, resuspension) processes, each contributing to the transformation and exchange of OM during transit (Raymond et al., 2004 and references therein). The content, composition and isotopic characteristics of OM ultimately discharged to the coastal ocean all reflect the net effect of these processes (Ludwig, 2001; Raymond et al., 2004). Elucidating the sources of suspended and sedimentary OM, as well as the processes responsible for their transformation in large river systems is thus crucial to better constrain the composition and fate of terrestrial OM that is ultimately exported to the marine realm. Most previous studies have focused on the lower reaches of river systems in order to quantify and characterize particulate OM exported at the outlet of the fluvial system (e.g. Wang et al., 2012; Tao et al., 2018). Fewer studies have addressed the basin-wide origin and extent of terrestrial OM processing within rivers (Freymond et al., 2018). Systematic investigation of the longitudinal evolution of OM characteristics of suspended and sedimentary OM is nevertheless essential to better understand those factors that influence the composition and fluxes of materials ultimately exported from a river basin.

The Pearl River, together with the Yangtze and Yellow rivers, transport 1.5 Pg sediment annually to the marginal seas of the northwestern Pacific, accounting for ~10% of global riverine sediment discharge (Milliman and Farnsworth, 2011). While several studies have investigated the sources and composition of particulate OM in the Yangtze and Yellow rivers (e.g. Wang et al., 2012; Li et al., 2014; Tao et al., 2018), the Pearl River has received less attention, despite it being the largest sediment source to the northern South China Sea (Liu et al., 2016). In addition, the Pearl River is influenced by intensive weathering and soil erosion as a result of large karst areas in the upper reaches, as well as intense human activity in the lower reaches (Luk et al., 1997). These factors all contribute to the nature and flux of riverine SPM and deposited sediments. Although a few recent studies have examined some aspects of the composition of suspended and sedimentary OM (He et al., 2010; Wei et al., 2010; Sun et al., 2015; Li et al., 2017; Liu et al., 2017), the sources and nature of particulate OM transported through and accumulating within this subtropical fluvial system remain poorly understood. Here, we investigate the composition and sources of OM for sediments along middle and lower reaches of the Pearl River system. Through integration with compiled available literature data on OM characteristics of SPM and soil profiles, we constrain provenance and alteration of suspended and sedimentary OM in the Pearl River system.

2. MATERIAL AND METHODS

2.1. Study area

In terms of annual water discharge and sediment load, respectively, the Pearl River (Fig. 1a) is the 2nd and 3rd largest river in China, and the 13th and 15th largest in the world. With a total drainage area of 0.80×10^6 km^2, the Pearl River consists of three major tributaries, West River (Xijiang), North River (Beijiang) and East River (Dongjiang) (Fig. 1b). The West River is the main tributary and originates from Maxiong Mountain with an elevation of 2444 m above sea level. This tributary has a total length of 2320 km and a catchment of 0.35×10^6 km^2, accounting for ~78% of the total drainage area and ~80–95% of the suspended sediment load of the Pearl River. The North and East rivers have drainage areas of 0.038×10^6 km^2 and 0.025×10^6 km^2, respectively, and originate from Damao and Yajibo Mountains with elevations of 500 m and 1102 m above sea level, respectively. The total lengths of North and East rivers are 573 km and 562 km, respectively.

Carbonate rock, ranging from Cambrian to Triassic in age, is widely exposed in the upper basin (Fig. 1c), covering a total area of 0.18×10^6 km^2 (Huang and Lin, 1983), and the resulting karst-dominated landscape is virtually devoid of soil and vegetation in several places. The middle and lower basins mostly consist of Precambrian metamorphic (schist and gneiss) and magmatic (mainly granite) rocks (Xu and Liu, 2010). Jurassic sedimentary rocks (shales and red sandstones) are also sporadically exposed in the middle basin (Li et al., 2014). Located in the humid subtropical region of South China, the Pearl River watershed has a mean annual air temperature of greater than 20 °C in the southeast region and between 12 °C and 18 °C in the northwest region (Huang and Lin, 1983). Annually, the Pearl River catchment receives 1500–2000 mm of precipitation in the southeast and 1000–1500 mm in the northwest. The vegetation types in the drainage basin are dominated by monsoon evergreen broadleaf rainforest (e.g. *Schima superba*, *Pinus massoniana*, *Cunninghamia lanceolate* and *Pinus elliotti*) with well-developed shrub and grass undergrowth (Luk et al., 1997). The Pearl River basin is dominated by lateritic "red earth" soils, while "yellow earth" soils occur in the middle basin, and paddy soils are abundant in the upper basin and the Pearl River delta (PRWRC, 1991).

2.2. Sampling

To provide an integrated assessment of carbon cycling in the Pearl River system, the sediment deposits were collected from its three tributaries. The results stemming from analysis of these samples were complemented with published data on SPM and soil profiles that were available from the Pearl River watershed.

2.2.1. Sampling of river sediments

In March 2004, prior to the onset of the wet season, we collected thirty-eight sediment samples deposited in the middle and lower reaches of the Pearl River. These samples were taken from the topmost horizon, either from the river flank near the high water-level or from the river bottom at shallow water depth (<1 m) along the course of the three

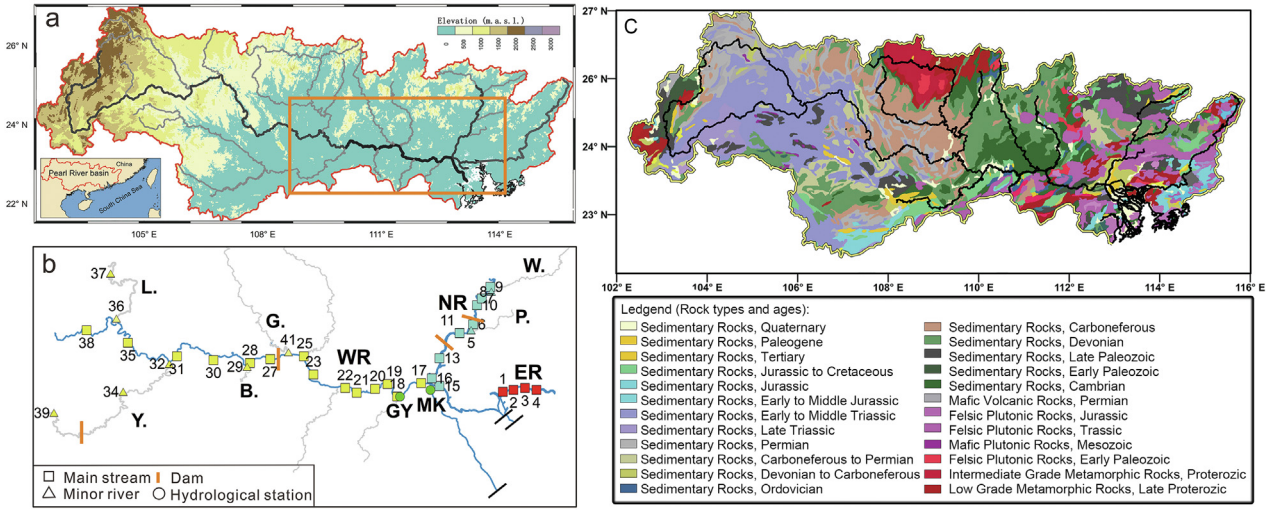

Fig. 1. (a) Map of the Pearl River watershed in South China, (b) locations of sediment samples investigated from its three major tributaries, West River (WR), North River (NR), and East River (ER), indicated by yellow, cyan and red color symbols, respectively, with sample numbers (Appendix B1), and (c) the geological map of the Pearl River watershed. Panel b is the enlarged view of the rectangle area marked in the Panel a. Location of four dams ('Changzhou' located in the West River, 'Xijin' in the Yujiang, and 'Feilaixia' and 'Shijiao' in the North River) are indicated by orange bars. Minor rivers, Luodinghe (LD.), Hejiang (H.), Guijiang (G.), Beiliujiang (B.), Yujiang (Y.), and Liujiang (L.) are joining to the West River, and Pajiang (P.) and Wengjiang (W.) connecting with North River. Two hydrological stations, Gaoyao (GY) and Makou (MK), in the Pearl River downstream are shown as green circles. In Panel c, all rocks are colored with age and sedimentary and metamorphic rocks are also differentiated. Bedrock age and rock type are from GeoMapApp (www.geomapapp.org).

major tributaries and their minor streams (Fig. 1b; Liu et al., 2007). The sampling sites were selected to avoid contamination from erosion of riverbank material as well as potential anthropogenic activity. There was no riverbank erosion detectable nearby all sampled sites; hence we infer that the collected sediments reflect deposition from the river water. To avoid potential anthropogenic contribution, all sampled sites were at least 1 km away from any village or human residence. All sediment samples were stored at 4 °C in sealed polyethylene bags until analysis.

2.2.2. Sampling methodologies for published data

Elemental and isotopic data of SPM compiled in this study were obtained primarily from samples collected in 2004 and 2005 (Wei et al., 2010; Sun et al., 2015). As our deposited sediments were sampled in the same period, this reduces biases introduced by the variable hydrological conditions in this river system. For the SPM sampling from March to December 2004, river water samples were collected monthly with volumes between ~0.3 L and ~6 L. Samples were obtained from ~0.5 m, 5 m (mid-depth) and 9.5 m (0.5 m above riverbed) below the surface, from the Makou hydrological station near the West River outlet (Fig. 1b; Wei et al., 2010). After that, river water from these three depths were mixed and then filtered through 0.7 μm glass fiber filters (Whatman GF/F, 47 mm). In 2005, the water samples were collected at 1 m below the water surface during wet (June and July) and dry (April and December) seasons along the lower reaches of the West River (Sun et al., 2015). After collection, the water samples were filtered through 0.7 μm GF/F filters. The SPM remaining on the filters was then stored frozen until further analysis.

The 2004 SPM data represent composite samples from three water depths in order to represent the overall characteristics of suspended OM composition in the Pearl River, while corresponding data from 2005 may not be fully representative of the average suspended load given that strong vertical gradients in suspended OM composition may exist (Galy et al., 2007; Bouchez et al., 2010, 2014). Nevertheless, representative SPM samples can be obtained during the wet season as high sediment discharge leads to high turbulence and mixing in the channel (Clark et al., 2013). Uncertainties in suspended OM composition that may occur for dry season SPM cannot be assessed in the present study but should be addressed in future studies.

The soils for which data have been collected are the yellow and red soils from southwest Guizhou, Maolan Natural Reserve Park of Hechi city, and Dinghushan Mountain in the Pearl River watershed (Fig. A4). The sites from which samples have been collected and for which OM composition was investigated were described by Shen et al. (2000, 2001), Chen et al. (2002a, 2002b), Zhu and Liu (2006) and Han et al. (2015) (Figs. A4 and A5). In southwest Guizhou and Maolan Natural Reserve Park, surface (0–10 cm) soil samples were taken, followed by samples from the walls of soil pits at 10 cm increments to depths of 70–210 cm (Zhu and Liu, 2006; Han et al., 2015). Five soil profiles with depth of 50–150 cm were excavated from Dinghushan Mountain (Shen et al., 2000, 2001; Chen et al., 2002a, 2002b). The top soil containing abundant plant debris and fine plant roots was removed and the underlying soil was subsampled at different intervals based on soil characteristics.

2.3. Analytical methods

Prior to the laboratory work, all sediments were oven-dried at 50 °C. Bulk sediments were soaked in 1 M hydrochloric acid (HCl) for 16 h at room temperature (25 °C) to remove carbonates and then rinsed three times with Milli-Q water to remove any trace of HCl. Approximately 20 mg of the decarbonated sediment was loaded into tin capsules and weight percentages of total organic carbon (TOC) and total nitrogen (TN) and stable carbon isotopic composition ($\delta^{13}C$) were determined using the elemental analyzer-isotope ratio mass spectrometry (EA-IRMS; Flash EA 1112 HT-Delta V Advantage). TOC data are presented on a carbonate-free basis. The analytical precision for TOC and TN is better than 0.01%. Stable carbon isotope results are reported in δ notation as the $^{13}C/^{12}C$ ratio relative to a standard (Pee Dee Belemnite) in per mil (‰). The analytical precision of $\delta^{13}C$ for our standard (acetanilide) is ±0.08‰. Low content of dolomite (<2%) is thought to be fully removed from the samples while rinsing with 1 M HCl and is unlikely to affect our data quality (e.g. Hemingway et al., 2018; supplementary material section A-2).

A portion of pre-weighed sediment (3–100 mg) was acid-fumigated in silver boats with 12 M HCl to remove carbonate at 60 °C and then neutralized over sodium hydroxide (NaOH) pellets to remove residual acid under the same temperature condition (Komada et al., 2008). The radiocarbon (^{14}C) content of these samples was measured by MICADAS accelerator mass spectrometer (AMS) interfaced with an elemental analyzer, at the Laboratory of Ion Beam Physics, ETH Zürich. Details of the instrumentation are described elsewhere (Synal et al., 2007; Wacker et al., 2010). The ^{14}C contents were corrected for the isotope fractionation during measurement using AMS-derived $\delta^{13}C$ values of each sample (Broecker and Olson, 1961). The results are reported as fraction modern (F_m) (Stuiver and Polach, 1977), which is defined as $^{14}C/^{12}C$ ratio of the samples deviating from that of the 95% of the radiocarbon concentration (in 1950) of NBC Oxalic Acid normalized to $\delta^{13}C$ of −19‰. The absolute error of F_m values for all samples is better than ±0.01. The conventional radiocarbon ages were calculated based on the equation: $t = -8033 \times \ln(F_m)$ expressed as years Before Present (yr BP, where present is 1950 AD) (Stuiver and Polach, 1977). Although two different acidification methods, HCl-rinsing and HCl-fumigation, were used to remove carbonate in sediments prior to $\delta^{13}C$ and $\Delta^{14}C$ measurement, respectively, potential biases introduced by these two acid pretreatments are considered negligible and do not significantly impact our conclusions (supplementary material section A-2).

After removing organic matter by oxidation at 350 °C in an oven for 12 h (Mayer, 1994b), surface area (SA, m^2/g) of sediments was measured with a NOVA 4000e surface area analyzer based on a 5-point nitrogen adsorption isotherm using the BET (Brunauer-Emmett-Teller) method

(Brunauer et al., 1938). Replicate analyses of two reference minerals (Quantachrome standards 2009 and 2007) generated values of 25.8 ± 0.14 ($n = 7$) and 2.72 ± 0.03 ($n = 6$) with consensus SA of 27.5 ± 3.6 m^2/g and 2.9 ± 0.2 m^2/g, respectively. After SA measurement, approximately 20 mg sediment was dispersed in an aqueous solution of sodium hexametaphosphate (1 g/L), ultrasonicated for 5 min, and then subsequently measured for grain size using a Malvern Mastersizer 2000.

3. RESULTS

Data on median grain size, mineral SA, weight percentages of TOC and TN, and stable and radiocarbon isotopic compositions ($\delta^{13}C$ and F_m) for Pearl River sediments obtained in this study are listed in Appendix B1. To facilitate the comparison of data from different stations within the Pearl River, stations from the main stream and from minor tributaries are identified in each figure.

3.1. Elemental and stable isotopic composition

The TOC content of riverine sediment samples ranges from 0.20 to 2.29%, with most values falling between 0.5 and 1.0% (avg.: 0.83 ± 0.46%; Fig. 2a). Higher TOC contents are, in general, associated with sediments collected from the upstream areas, whereas two sediment samples collected in between dams of the North River show relatively low TOC content (Fig. 2a). The TN content ranges from 0.03 to 0.23% and correlates positively with the TOC content ($R^2 = 0.85$; Fig. A2). Atomic C/N ratios vary between 6.5 and 19.6 (Fig. 2b). For most fluvial sediments, C/N ratios are greater than 10, except for those samples collected either upstream of or between dams, which show lower C/N ratios (6.6–8.9). The $\delta^{13}C$ values for TOC vary from −25.7 to −20.2‰ (Fig. 3a), with higher values mostly seen in the upstream sediments. The range of $\delta^{13}C$ values of sediments from the North and East rivers overlay with reported $\delta^{13}C$ ranges for river sediments at the outlet of these rivers (East River: −26.1 to −23.1‰, $n = 8$, He et al., 2010; North River: −29.0 to −20.6‰, $n = 13$, Li et al., 2017). The present study reports the first data on OM composition of surface sediments from the West River, which is responsible for ~90% of overall Pearl River sediment discharge (Figs. 6 and 7, the Ministry of Water Resources of the People's Republic of China, MWR, PRC, 2002, 2003, 2004, 2005).

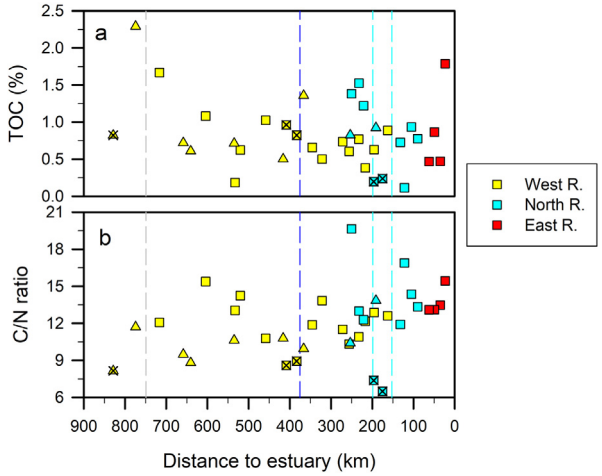

Fig. 2. Spatial variations of (a) TOC contents, and (b) atomic C/N ratios in sediments, as a function of distance to the Pearl River estuary. The distance to estuary is estimated by measuring the distance from the sampling site to the outlet of each river (marked by a black line in Panel b; Fig. 1) in Google Earth. Vertical dashed gray, blue and cyan lines mark the location of dams along the Yujiang, West River and North River, respectively (see Fig. 1b). The symbols with triangle represent the samples from minor rivers and symbols with "×" represent the samples investigated either upstream to a dam or in between two dams.

3.2. Radiocarbon activity

The F_m values for TOC in the sediments of Pearl River range from 0.38 to 1.10, corresponding to conventional radiocarbon ages between modern and 7878 yr BP. They generally fall in a lower range than those for SPM in the same river (Wei et al., 2010). F_m values in the sediments do not show any spatial variation from upstream to downstream. The F_m values of the West River sediment vary between 0.38 and 0.94, corresponding to radiocarbon ages of 508 and 7878 yr BP (Fig. 3b). This range is wider than the range of F_m reported for SPM (0.58–0.90; Wei et al., 2010; Liu et al., 2017). In addition, the F_m values in the West River sediments are positively correlated with the C/N ratios ($R^2 = 0.68$; Fig. 9). The F_m values of North River sediment range from 0.41 to 1.01 (7153 yr BP to modern). This range is more variable than that of F_m values reported for wet season SPM in this river (0.75–0.82; Wei et al., 2010). The F_m values in the East River sediment vary from 0.51 to 0.80 (1378 to 5387 yr BP) and these values are substantially lower than the F_m values reported for SPM collected from the Boluo hydrological station in the same river (0.82–0.94; Wei et al., 2010). The range of F_m for SPM (0.58–0.94) and sediment (0.38–1.01) in the Pearl

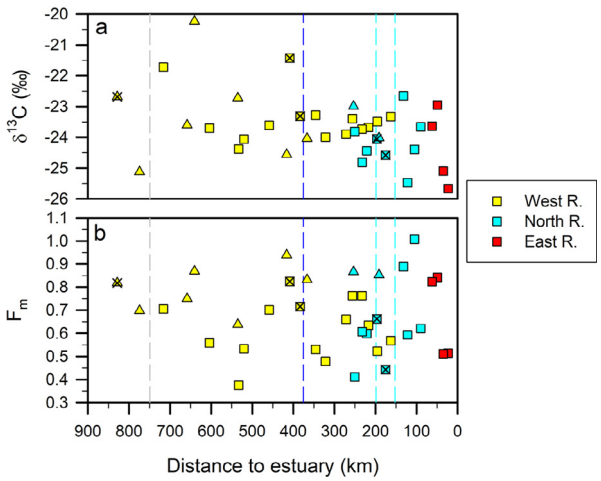

Fig. 3. Spatial distributions of (a) $\delta^{13}C$, and (b) F_m in sediments investigated along the Pearl River system. For the additional details of vertical lines and symbols, refer to Fig. 2 caption.

River is higher and more variable than those reported for SPM from other large river systems such as the Amazon (0.37–0.86; Bouchez et al., 2014), the Yellow (0.37–0.60; Wang et al., 2012; Tao et al., 2018), and the Yangtze (0.29–0.57; Li et al., 2014).

3.3. Grain size and OC loading

With the exception of two samples (PR33 and PR14, see Appendix B1 and Fig. 1b), the Pearl River is dominated by fine-grained sediments with mud (clay + silt) content ranging from 62 to 98% (Fig. 4a). These two outliers are dominated by an exceptionally large sand fraction (93% and 73%, respectively) and reflect a clearly different depositional or erosional regime, and are therefore excluded from further discussion and from Figs. 4 and 5. The median grain size for all samples ranges from 7 to 37 μm (Fig. 4b), while mineral SA ranges from 11.8 to 37.8 m^2/g and is negatively correlated with median grain size (Fig. 4c and 5a). OC-loadings (OC/SA ratios) range from 0.10 to 1.14 mg C/m^2. Most investigated sediments plot in the zone below 0.4 mg C/m^2, though two samples plot the area above 1.0 mg C/m^2 and few samples fall in between (Fig. 4d and 5b). The OC loading generally decreases from

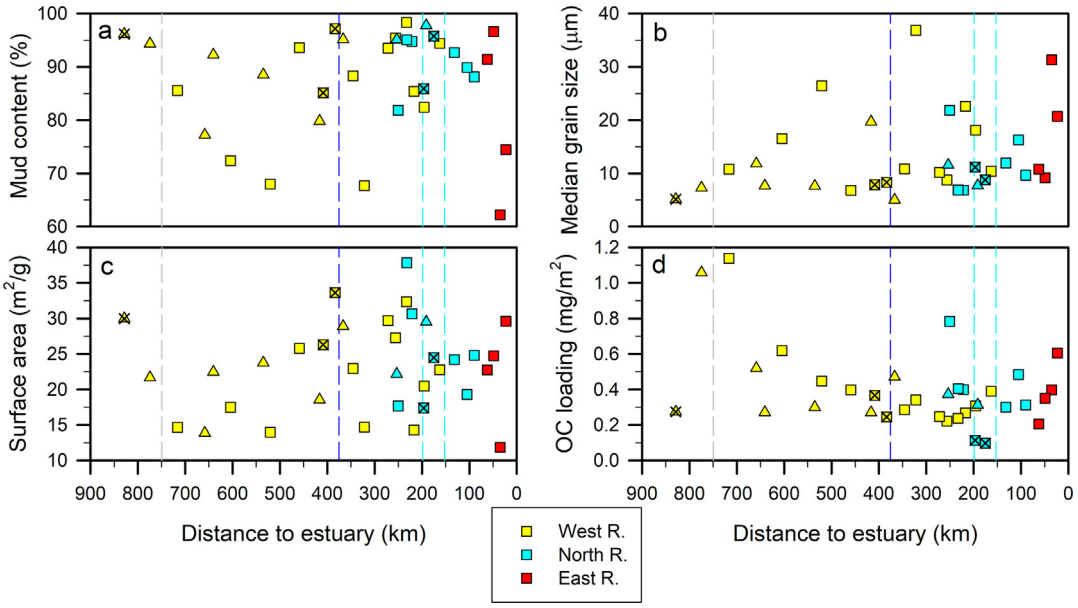

Fig. 4. Spatial distributions of (a) mud content (clay + silt), (b) median grain size, (c) mineral surface area, and (d) OC loading in sediments along the Pearl River. For details of vertical lines and symbols, refer to Fig. 2 caption.

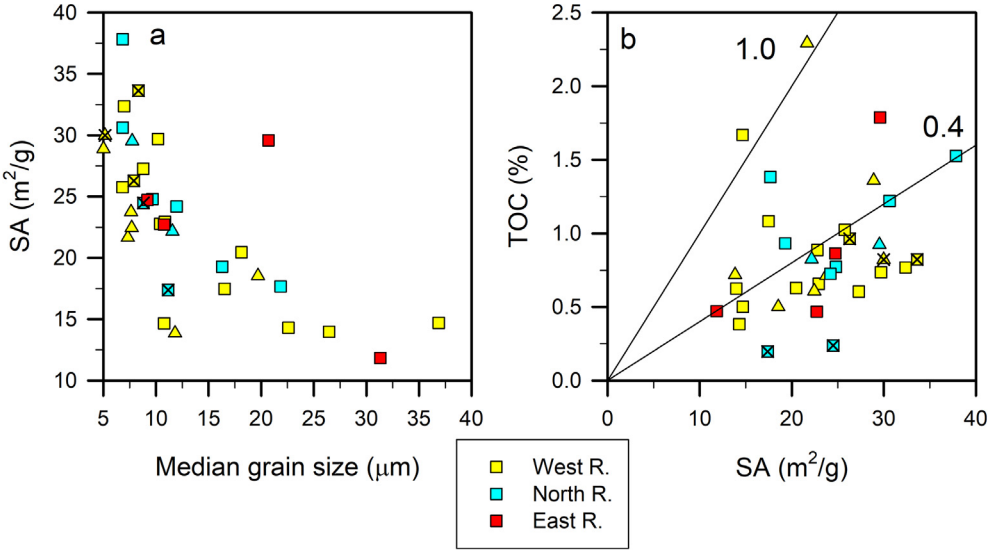

Fig. 5. (a) Surface area (SA) versus median grain size, and (b) TOC contents as a function of their mineral SA in sediments of the Pearl River. The zone spreads between 0.4 and 1.0 m^2/g in the plot is the monolayer equivalent (ME) level proposed by Mayer (1994b). For the additional details of vertical lines and symbols, refer to Fig. 2 caption.

the upstream towards downstream, with sediments collected between dams in the North River exhibiting markedly lower OC loadings (Fig. 4d).

4. DISCUSSION

4.1. Riverine sediment transport

Transport and deposition of sediments within modern-day river systems are controlled by hydrological regime and human activity (Wu et al., 2012). Human activity has increased sediment transport by exacerbating soil erosion, but reduced the flux of sediment reaching the coastal zone due to impoundments (Syvitski et al., 2005). In the Pearl River, most of the sediment transport takes place during the wet (monsoonal) season with large water fluxes (Fig. 6). Sediment deposition is thought to occur on river flanks during periods of elevated water discharge or in shallow, hydrologically quiescent locations during decreasing water level after a high-discharge event. The annual

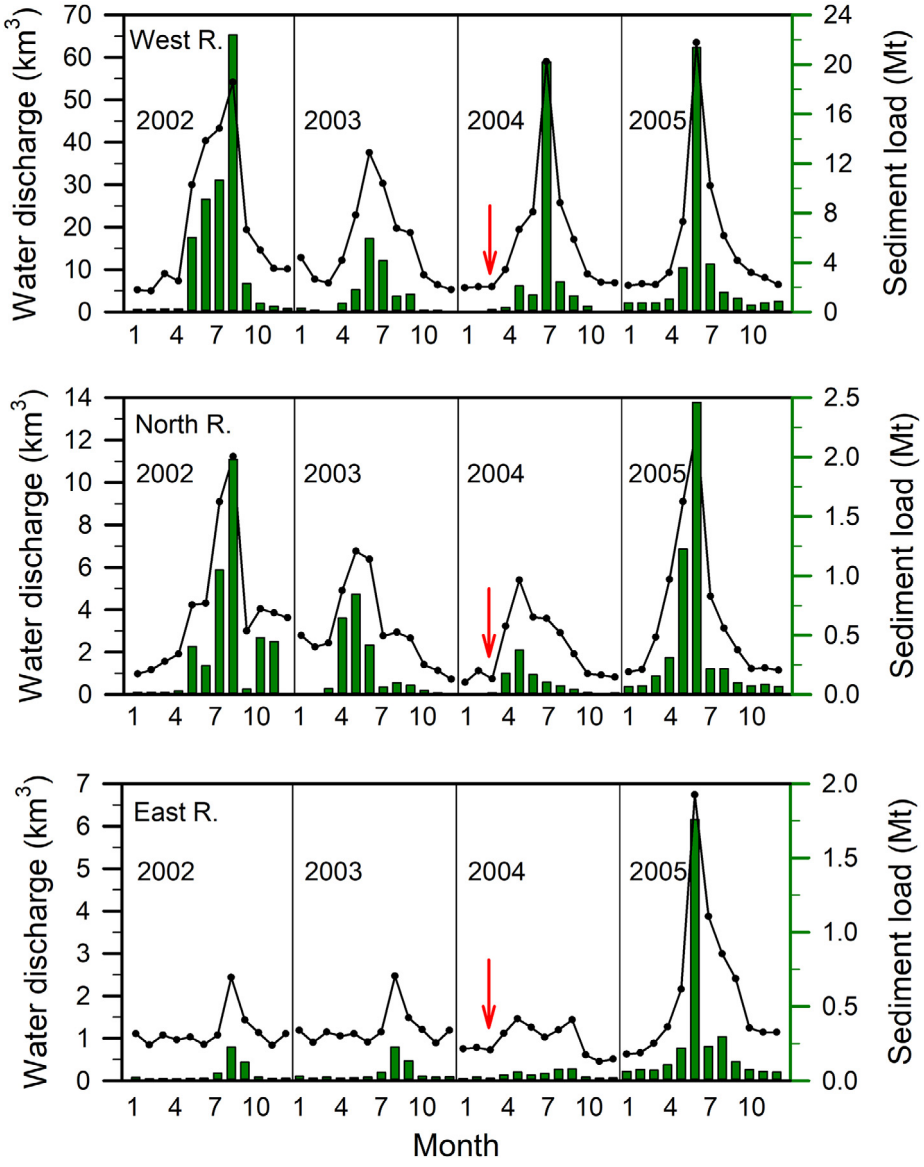

Fig. 6. Temporal variations in water discharge (black lines) and sediment load (green bars) recorded at hydrological stations, Gaoyao, Shijiao and Boluo, in the West, North and East rivers, respectively, in the lower reaches of the Pearl River during 2002–2005 (MWR, PRC, 2002, 2003, 2004, 2005). The red arrow indicates the sampling time of sediment samples investigated in this study. The seasonal variations of water discharge and sediment load in the years of 2003 and 2004 clearly illustrate that our samples were collected during relatively low water level and low sediment load conditions. The Pearl River experiences a subtropical and tropical monsoon climate. According to the MWR, PRC report, the Pearl River watershed was relatively dry in 2003, which is thought to be related to a moderate El Niño occurring in that year (NOAA, https://ggweather.com/enso/oni.htm). Most of the sediments investigated in this study are therefore likely to have been deposited during the period of high water and high sediment flux in 2002, in that year, the Pearl River experienced high water and high sediment discharge from May to August. These enhanced fluxes are probably related to a weak La Niña in the first half of the year.

sediment load recorded from 2002 to 2005 in Pearl River shows the enhanced sediment fluxes in the middle and lower reaches compared to the upper reaches (Fig. 7), indicating that large amounts of SPM is derived from the mid- and downstream regions. In addition, these high suspended loads occur in mid- and downstream waters predominantly during the wet season due to soil erosion/mobilization (Figs. 6 and 7; Wu et al., 2012). In the monsoon-dominated Pearl River, precipitation and associated fluxes of water and suspended sediments were high during 2002, but relatively low in 2003 (Figs. 6 and 7). Consequently, our sediment samples taken prior to the 2004 summer monsoon are likely to have been deposited during the high water and sediment discharge in the rainy season of 2002, while minor contributions during 2003 and 2004 are also possible. Thus, the provenance of river sediment is linked to wet-season soil erosion, which is discussed further in the following section. We focus on OM-related processes and provenance for the mid- and downstream Pearl River sediments, in particular on the West River because it dominates the annual sediment flux. In addition, West River has the most complete and comprehensive datasets of elemental and isotopic compositions on soil OM and suspended OM.

A number of processes can contribute to suspended and sedimentary OM in the Pearl River, including chemical and physical weathering of bedrock (petrogenic OC), soil erosion, entrainment of recent vegetation/plant debris, and in-situ aquatic primary and secondary productivity. We therefore focus on potential OM sources and their controlling mechanisms using C/N ratio, $\delta^{13}C$ and F_m values (e.g. Chen et al., 2002a, 2002b; Alin et al., 2008; Goñi et al., 2014; Blattmann et al., 2019), in order to better constrain OM provenance and modification in Pearl River suspended and deposited sediments. Given the non-conservative behavior of OM during mobilization, transport and temporary storage (Raymond et al., 2004 and references therein), tracing and quantifying the OM provenance in suspended and deposited sediments requires knowledge of both probable sources and the processes that alter their biogeochemical fingerprints.

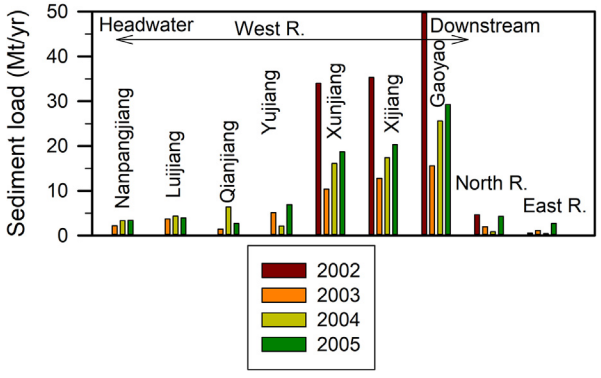

Fig. 7. Spatial variation of sediment load recorded at different hydrological stations along the Pearl River from the headwater to the downstream during 2002–2005 (MWR, PRC, 2002, 2003, 2004, 2005). Higher sediment loads were found in the middle and lower reaches, Xunjiang, Xijiang and Gaoyao, relative to the upper reaches, Nanpanjiang, Liujiang, Qianjiang and Yujiang during 2002–2005, suggesting the remobilization of soil predominantly from the middle and lower Pearl River basin.

4.2. Sources of riverine dissolved inorganic carbon

In view of rapid soil OM degradation rates and relatively short anticipated river-water residence times, remineralization of recent, labile soil OM is likely to contribute significantly to riverine DIC (Raymond et al., 2004; Sun et al., 2015). In contrast, the residual refractory soil OM comprises the main component for SPM and sediment deposits in the Pearl River (supplementary material section A-4). In addition to soil CO_2 derived from the degradation of soil OM, other potential sources of riverine DIC (which is composed of bicarbonate (HCO_3^-), carbonate (CO_3^{2-}) and dissolved carbon dioxide (CO_2)) include bicarbonate from dissolution of carbonate and silicate rocks, and atmospheric CO_2 that exchanges with river water (Yang et al., 2016). As each of these sources carry distinct $\delta^{13}C$ and F_m signatures, their respective contributions to DIC can be derived by applying a simple dual mass balance using end-member values for each sources and measurements on Pearl River DIC (supplementary material section A-4).

The average contributions to annual riverine DIC from soil CO_2, weathering and atmospheric interaction are $35 \pm 5\%$, $42 \pm 15\%$ and $23 \pm 20\%$, respectively (Table 1). The riverine primary productivity, a major OM fraction for dry season SPM (Sun et al., 2015), has a negligible effect on the DIC content and composition during all seasons (supplementary material section A-4). Irrespective of dry-wet-flood runoff conditions, the relative contribution from source-rock weathering is rather constant (Table 1). However, the DIC derived from soil-OM degradation is the greatest when higher amounts of soil are mobilized during wet and flood seasons (Table 1). It is inferred that enhanced soil erosion exposes more soil OM to oxygen, thereby enhancing degradation and hence DIC production (Doetterl et al., 2016). In contrast, the reduced river water residence time during the wet season or flood event causes limited air-water gas exchange and thus limits the contribution from atmospheric CO_2. The longitudinal evolution of DIC isotopic characteristics along the river, after the initial major contribution from rock weathering, is mainly

Table 1
Proportional fractions of soil, weathering and atmospheric CO_2 to dissolved inorganic carbon (DIC) sampled during the wet season, dry season, and flood event.

	Soil % Mean (Range)	Weathering % Mean (Range)	Atmosphere % Mean (Range)
Dry DIC	31 (29–33)	48 (40–58)	21 (9–31)
Wet DIC	39 (38–40)	43 (34–57)	18 (3–29)
Flood DIC	45 (42–49)	47 (35–58)	8 (0–23)
Total DIC	35 (29–40)	42 (31–60)	23 (0–41)

These fractions were calculated based on the $\delta^{13}C$ and F_m values of the DIC from Sun et al. (2015) and Liu et al. (2017). Refer supplementary material section A-4 for more details.

controlled by contributions from soil. This indicates that the degradation of labile soil OM is an important process within the river system. This process not only influences the isotopic composition of DIC, but also controls the composition of suspended and sedimentary OM.

4.3. Nature of OM sources

4.3.1. Vegetation-sourced OM

During surface run-off and soil erosion, modern vegetation-sourced OM may be entrained into the fluvial network. Recently synthesized OM will reflect the modern atmospheric ^{14}C levels, while corresponding $\delta^{13}C$ values of biomass primarily reflect different photosynthetic carbon fixation pathways (i.e. C3 vs. C4) and atmospheric CO_2. Additionally, small isotopic variation also occurs owing to different forms of vegetation (herb, fern, tree, shrub, sedge, etc.) and habitats (open, intermediate- and open-canopy sites). F_m values of leaves or grass grown between 2002 and 2004 must be close to that of atmospheric CO_2 with F_m of 1.07 ± 0.01 (Table 2; Fig. A3), while $\delta^{13}C$ measurement on Dinghushan forest vegetation sampled in the 1980s showed wide ranges from −34.9 to −26.4‰ (−30.2 ± 2.1‰, $n = 94$), and from −15.2 to −10.3‰ (−12.1 ± 1.1‰, $n = 34$) for the C3 and C4 plants, respectively (Ehleringer et al., 1987). Different $\delta^{13}C$ signatures of these plants and their distribution in the river basin are the major factor determining the $\delta^{13}C$ of underlying topmost soil OM (Zhu and Liu, 2006). The foliage in the lower basin showed an OC content of 48.4 ± 3.9%, and C/N of 34.9 ± 9.7 ($n = 33$; Fang et al., 2011). Large rivers receive leaf and woody debris associated with erosion of litter and soils from the upstream and/or riparian zone. During their downstream transport, labile components are subjected to rapid decomposition and diminution into finer particles, while more refractory constituents (e.g. lignin) may persist (Hedges et al., 1997).

4.3.2. Soil OM

Within the Pearl River watershed, several studies have reported OC content, C/N ratios, and $\delta^{13}C$ and F_m values of OM in soil profiles, but all parameters are rarely studied for the same sample/site (Shen et al., 2000, 2001; Chen et al., 2002a, 2002b; Zhu and Liu, 2006; Shen et al., 2012; Han et al., 2015; Sun et al., 2015; for details, see Figs. A4 and A5). In order to understand the nature of soil OM and processes that influence OM composition of riverine SPM and sediment deposits, we use two soil profiles to highlight general features that are representative of available soil data from the middle and lower reaches (Fig. 8). One is from Guizhou in the middle reaches, and the other is from Dinghushan in the lower reaches (Figs. 8, A4 and A5).

In the soil profile SL from Dinghushan, the OC content decreases rapidly with depth. F_m values are virtually constant in the upper few centimeters, suggesting the dominance of reactive modern OM that is rapidly degraded with depth. In general, the degradation rate of soil OM is age-dependent with recently formed OM being most rapidly degraded (supplementary material section A-3; Janssen, 1984; Middelburg, 1989). Clearly, both the soil OC content and F_m are diagnostic tracer of OM degradation processes. For this site, the turnover rate, i.e. the average time required to renew the content of the soil OM at steady state, of top soil OM is less than 10 years (Chen et al., 2002a, 2002b), while the degradation rate of soil OC is 0.36 yr^{-1} (Fig. A7). The rapid decrease in soil OC content from 5.5% to 1.4% is accompanied by a shift in $\delta^{13}C$ change from −27.0‰ to −20.1‰, indicating the preferential degradation of $\delta^{13}C$-depleted OM (−29.5‰; Fig. 8). For this profile, the F_m value for degrading soil OM is estimated at 1.11, which is similar to that of the atmospheric CO_2 (F_m: 1.10) in the sampling year (1998; Fig. A3), confirming the preferential degradation of modern OM. We observed a similar soil profile at YSS from Guizhou, but with different OM

Table 2
Means and ranges of TOC content, $\delta^{13}C$, C/N ratio and F_m of OM in sediment, wet and dry season suspended particulate matter (SPM), different soil components, C3 and C4 plants and phytoplankton in the Pearl River watershed.

	TOC % Mean ± SD (Range)	$\delta^{13}C$ ‰ Mean ± SD (Range)	C/N ratio (atomic) Mean ± SD (Range)	F_m Mean ± SD (Range)
Sediment	0.77 ± 0.35 (0.18–1.67)	−23.4 ± 0.8 (−24.4 to −21.4)	11.9 ± 1.9 (8.6–15.4)	0.62 ± 0.13 (0.38–0.82)
[*]Wet season SPM	1.43 ± 0.18 (1.12–1.83)	−23.3 ± 0.4 (−23.8 to −22.2)	12.9 ± 0.8 (11.6–14.7)	0.75 ± 0.09 (0.64–0.87)
[*]Dry season SPM	1.90 ± 0.65 (1.26–3.23)	−25.1 ± 0.9 (−26.2 to −23.5)	9.1 ± 1.3 (7.1–11.0)	0.65 ± 0.06 (0.58–0.72)
[a]Degrading soil		−27.7 ± 2.4 (−31.6 to −25.4)	15.8 ± 1.1 (15.0–16.6)	1.19 ± 0.07 (1.11–1.28)
[b]Top soil	2.41 ± 1.23 (1.26–5.09)	−24.2 ± 2.0 (−27.5 to −21.3)	12.9 ± 1.8 (11.6–14.1)	1.08 ± 0.09 (0.98–1.21)
[c]Top 100 cm soil	1.52 ± 0.85 (0.65–3.33)	−23.9 ± 2.0 (−27.5 to −21.1)	11.0 ± 1.5 (9.9–12.1)	1.00 ± 0.07 (0.91–1.09)
[d]Subsoil	0.82 ± 0.51 (0.35–1.86)	−23.2 ± 2.2 (−27.4 to −20.6)	6.6 ± 3.0 (4.4–8.7)	0.87 ± 0.13 (0.73–1.07)
[e]Deep soil	0.66 ± 0.41 (0.22–1.51)	−24.2 ± 1.9 (−28.0 to −21.7)	5.7 ± 3.2 (3.4–8.0)	0.74 ± 0.07 (0.66–0.80)
[f]C3 plant	48.35 ± 3.95 (38.5–54.6)	−30.2 ± 2.1 (−34.9 to −26.4)	34.9 ± 9.7 (16.5–66.8)	1.07 ± 0.01
[f]C4 plant		−12.1 ± 1.1 (−15.2 to −10.3)		
[g]Phytoplankton		−30.0 ± 1.1		0.86 ± 0.04

[*] The data are from Wei et al. (2010) and Sun et al. (2015) and shown in Appendix B3. a–e represent different soil OM components that are derived by averaging the compositions from 8 representative soil profiles (Appendix B2) that computed in the OC-weighted average basis. Refer to Section 4.3.2 for more details. Data sources are from Shen et al. (2000), Shen et al. (2001), Chen et al. (2002a, 2002b), Zhu and Liu (2006) and Han et al. (2015). [f] The data are from Ehleringer et al. (1987) and Fang et al. (2011). [g] The standard deviations for $\delta^{13}C$ and F_m of phytoplankton are assumed to be similar to those of dissolved inorganic carbon (Section 4.3.3).

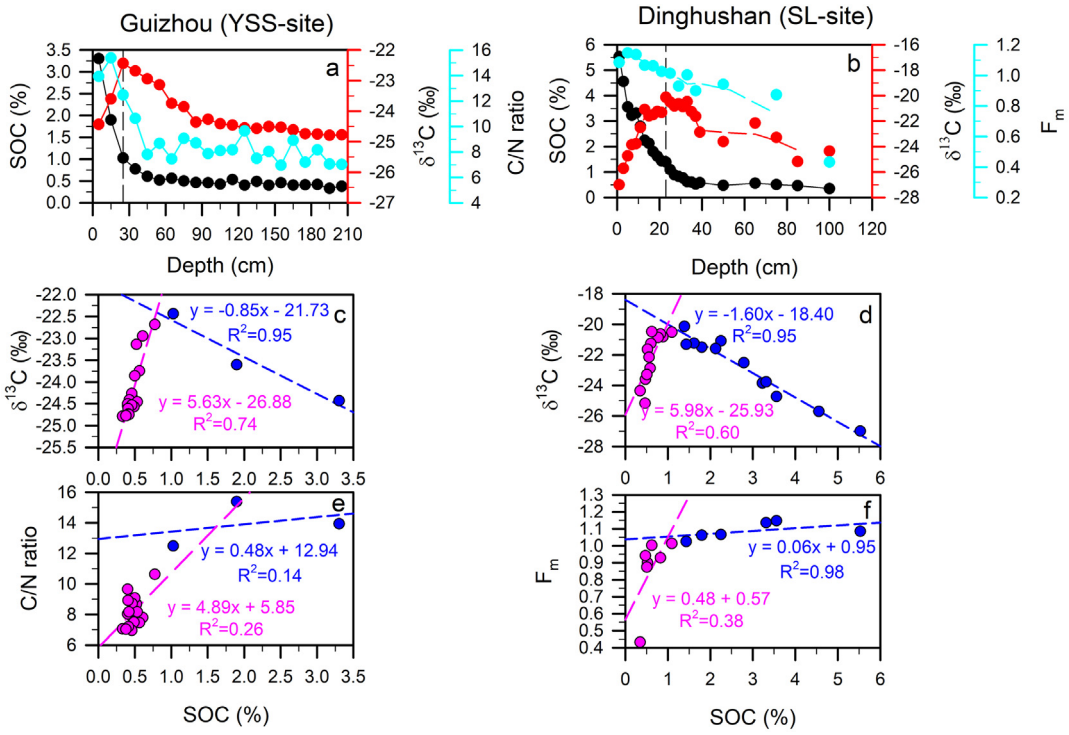

Fig. 8. (a and b) Depth profiles of soil organic carbon (SOC) content, C/N ratio, $\delta^{13}C$ and F_m, and (c–f) SOC content as a function of $\delta^{13}C$, C/N ratio and F_m, in soil from Guizhou (YSS-site, left panels) and Dinghushan (SL-site, right panels). Red and cyan dashed lines in Panel b are 3-point moving average. The black dashed line in Panels a and b marks the depth with highest $\delta^{13}C$, which is the boundary between rapidly degrading upper-layer and slowly degrading lower-layer soils. These two profiles, with the other 6 similarly shaped profiles (Fig. A5), are thought to be formed naturally and taken as representative soil profiles that used for studying the soil OM characteristics. Although the YSS profile does not have the same resolution as SL for the top soil, it is representative for an area with yellow soil that having similar shape. Unfortunately, there is no F_m for YSS and for SL and no C/N data for SL-sites. The blue and pink dots in Panels c-f represent rapidly and slowly degrading OM, and blue and pink dashed lines in these panels indicate a linear correlation. The average OM composition of the degrading component for each profile in the top soil can be derived from these correlations. For example, the $\delta^{13}C$ and F_m for the most labile OM in top soil for SL are changing from 5.5‰/−27.2‰ to 1.4‰/−20.6‰. Assuming a 2-component mixing system, we obtain $\delta^{13}C$ of −29.5‰, and F_m of 1.11 for the rapidly degrading OM component. Data sources are from Shen et al. (2000), Shen et al. (2001), Chen et al. (2002a, 2002b) and Zhu and Liu (2006).

characteristics for the degrading fraction ($\delta^{13}C$: −25.4‰, C/N ratio: 15.0; F_m not available). By averaging data for all eight, similarly-shaped soil profiles from middle and lower reaches (Fig. A5; Appendix B2), we estimate that the composition of the labile OM that is rapidly being decomposed (defined here as 'degrading soil OM') has $\delta^{13}C$ values ranging from −31.6 to −25.4‰ (−27.7 ± 2.4‰), C/N ratios from 15.0 to 16.6 (15.8 ± 1.1) and F_m values from 1.11 to 1.28 (1.19 ± 0.07) (Table 1). This rapid degradation represents more than 80% of the OM that is initially present in the topmost soil.

In contrast to rapid OM degradation rates in the top soil, the OM in deep soil (below 75 and 38 cm for the YSS and SL-site profiles; Fig. 8) is much more refractory. This refractory deep soil is characterized by low OC content, relatively constant $\delta^{13}C$ values and C/N ratios, and slowly decreasing F_m values with depth. The degradation rate of soil OM for this layer is <0.0003 yr^{-1} (Fig. A7). There is the moderately degradable OM fraction (probable turnover rate: ~100–500 yr) between the rapidly degradable (<10 years, top soil) and the refractory (>1000 years, deep soil) OM (Chen et al., 2002a, 2002b; Fig. A7). Our estimation of soil OM composition is based on eight soil profiles (Fig. A5) in the catchment that have considerable spatial variation in SOC content, C/N ratio, $\delta^{13}C$ and F_m. Among them, five soil profiles are from Dinghushan and this may bias the average composition of soil OM towards this site. One would expect a large heterogeneity in soil OM composition, and in turn soil OC degradation rates, in a large drainage basin such as the Pearl River. We therefore consider average composition of soil OC as a first-order assessment to best approximate this catchment-wide signal. The soil profile-derived degradation rate for OM is likely to be controlled to some degree by oxygen limitation. The sudden exposure of subsoil OM to surface oxic conditions during erosion enhances the degradation rate of subsoil OM (Doetterl et al., 2016). Soil OM degrades continuously for thousands of years under oxic conditions (Prahl et al., 2003; Huguet et al., 2008). During erosion and transport, the rapid degradation of the most labile soil OM allows the moderately degradable and refractory soil OM to dominate in river suspended and deposited sediments.

4.3.3. Riverine primary productivity

Riverine primary productivity (R_{pp}) includes OM synthesized by phytoplankton, benthic algae, aquatic vascular plants and mosses. In the Pearl River, the reported average concentration of chlorophyll *a* is 6.3 mg/m^3 and the average phytoplankton biomass is 2.6×10^6 cell/L (Yang et al., 2016), suggesting intense aquatic photosynthesis. The average F_m for the aquatic plants, including *Potamorgeton intortifolius*, *Hydrilla verticillata*, *Vallisineria spiralis*, *Ranunculus bungei Steud*, and *Spirogyra*, in the Pearl River was reported to be 0.83 ± 0.08 ($n = 8$; Liu et al., 2017). Other than this, there is no data on TOC and TN contents, $\delta^{13}C$ or F_m values reported for the phytoplankton in the Pearl River.

Generally, the freshwater algae contain low C/N ratios between 4 and 8 due to their high protein content (Meyers, 1994). The isotopic composition of R_{pp} ($\delta^{13}C$ and F_m) depends not only on the composition of DIC, but also on fractionation processes during DIC uptake (Fry and Sherr, 1989). The fractionation is mainly dependent on species, dissolved CO_2 concentration and temperature (Rau, 1994), and is generally thought to fall in the same range as marine phytoplankton, i.e. −18 to −22‰. Given ambient temperatures in the Pearl River system, this isotopic fractionation likely to fall in the lower end of this range (i.e. −19/−20‰). The $\delta^{13}C$ values of DIC range from −8.5 to −11.4‰ in the West River downstream (−10.1 ± 1.1‰; Sun et al., 2015). Accordingly, the R_{pp} is expected to have a $\delta^{13}C$ of ~−30.0‰, similar to a measured average $\delta^{13}C$ value of R_{pp} in the Maotiao River (−29.1‰; Li, 2009), an upstream tributary of Yangtze River located close to the West River upstream. The F_m of DIC for the Pearl River ranges from 0.81 to 0.96 (0.90 ± 0.04) (Liu et al., 2017). During DIC uptake, the biota preferentially utilizes light ^{14}C, resulting in ~40‰ fractionation for $\Delta^{14}C$ relative to DIC. Therefore, the F_m for R_{pp} is expected to be ~0.86, which is similar to the F_m reported for Pearl River aquatic plants (0.83 ± 0.08; Liu et al., 2017). Even though the OM produced in situ tends to be more susceptible to rapid turnover, a fraction will also contribute to the particulate OM in the fluvial system (Blair et al., 2004).

4.4. Provenance of suspended and sedimentary OM

The vegetation, soil and bedrock are eroded and entrained to the river from the watershed, and subsequently either transported as suspended sediment and/or bedload, or deposited on the river flank (floodplain) or riverbed. During these transfers, the OM is not conservatively transported; instead it is subjected to alteration by a series of dynamic processes (i.e. degradation or addition of certain OM components). Here we compare the OM composition of SPM and sediment deposits with that of potential OM sources, to evaluate ensuing processes and to determine their provenance.

4.4.1. Suspended particulate matter

Wet season SPM is reported to be predominantly soil-derived (Wei et al., 2010; Sun et al., 2015). If we assume that the top 100 cm of soil is eroding into the river, and there is negligible input of other material and no degradation during transport, then the resulting SPM would have an OM composition that is similar to the weighted average of this upper 100 cm of soil. Averaging the top 100 cm soil OM component from 8 profiles gives $1.52 \pm 0.85\%$ OC, -23.9 ± 2.0‰ $\delta^{13}C$, 11.0 ± 1.5 C/N ratio, and 1.00 ± 0.07 F_m (Table 2; Section 4.3.2). Even though the thickness of eroded soil is variable and unknown, the integrated OM composition for any thickness of upper soil is less variable because the surface soil contains the majority of the OC. The composition of wet season riverine SPM is $1.43 \pm 0.18\%$ OC, -23.3 ± 0.4‰ $\delta^{13}C$, 12.9 ± 0.8 C/N ratio, and 0.75 ± 0.09 F_m (Table 2). Thus, the OC content, $\delta^{13}C$ values and C/N ratios of the latter are consistent with the integrated values of the top 100 cm of soil, while corresponding F_m values differ markedly (1.00 ± 0.07 vs. 0.75 ± 0.09).

A significant contribution from vegetation can be excluded based on their high F_m values (F_m: 1.07 ± 0.01; Section 4.3.1). The soil OM remaining after the rapid degradation of the recently formed OM in the top soil (defined as subsoil) is thought to be most relevant to SPM on the time scale of the riverine processes. The degradation of labile OM of the top soil is consistent with the enhanced contribution from soil CO_2 to DIC during the wet season and flood events (Section 4.2). The subsoil can be represented by the top 100 cm soil after removal of the labile OM in the top soil. This subsoil OM contains $0.82 \pm 0.51\%$ OC, -24.2 ± 2.0‰ $\delta^{13}C$, 6.6 ± 3.0 C/N ratio, and 0.87 ± 0.13 F_m (Table 2). However, this is also inconsistent with the OM composition of wet season SPM. Potential R_{pp} inputs enhance the OC content but corresponding F_m values are too high to explain the low F_m in the wet season suspended OM (0.86 ± 0.04 vs. 0.75 ± 0.09). Moreover, this freshly formed OM is prone to relatively rapid degradation. The addition of (re-) mobilized sediment containing a higher fraction of refractory soil OM or from petrogenic OC being devoid of ^{14}C might explain the low F_m values. Consequently, several processes are required to explain the OM compositional variability of wet season SPM.

4.4.2. Sediment

The sediments are thought to be mainly deposited during the wet season when both water and sediment discharge are high. Most of this supply comes from eroded soil, but with a potential contribution of OM from R_{pp}. The OC content, $\delta^{13}C$, C/N ratio and F_m values for sediments are $0.77 \pm 0.35\%$, -23.4 ± 0.8‰, 11.9 ± 1.9, and 0.62 ± 0.13, respectively (Table 1). The C/N ratio and $\delta^{13}C$ values for this sedimentary OM are similar to those of wet season SPM (Table 2). However, the sediment contains much lower OC contents and lower F_m values and thus is older than the SPM. This suggests that the OM fraction that dominates the sediment after a certain period of emplacement is more refractory OM, likely sourced from deep soil. The refractory OM from deep soil for the 8 profiles contains $0.66 \pm 0.41\%$ OC, with $\delta^{13}C$, C/N and F_m values of -24.2 ± 1.9‰, 5.7 ± 3.2, and 0.74 ± 0.07, respectively (Table 2). Compared to deep soil, sediment contains slightly

higher OC contents and $\delta^{13}C$ values, but lower F_m and a significantly higher C/N ratio.

The compositional discrepancy between deep soil and sediment may be explained by OM contributions from R_{pp} and ancient bedrock, and associated degradation and preservation processes. The addition of R_{pp} would result in higher OC content and F_m values, and lower $\delta^{13}C$ values, while degradation of OM would increase the C/N ratio due to preferential degradation of more labile organic nitrogen components (Fig. 9). Overall, however the contribution of R_{pp} would only slightly increase the F_m because most of that fraction would be degraded, while inputs of deeper soil with low F_m and OC contents can be excluded because of their extremely slow degradation rates ($0.0002\ yr^{-1}$). A minor contribution of petrogenic OC with low OC content will decrease the average F_m and OC content of the sediment. Therefore, instead of a simple conservative mixing of potential OM sources, mixed contributions from deep soil, R_{pp} and petrogenic OC, as well as subsequent degradation processes, must be considered in order to explain the composition of sedimentary OM.

4.5. Quantifying sources for suspended and sedimentary OM

Suspended and sedimentary OM both consist of varying contributions from autochthonous (in-situ produced R_{pp}) and allochthonous components with the latter comprising a mixture of eroded soil and bedrock (petrogenic) OC from the catchment (Fig. 10a). Here, we quantify the proportional contribution of these sources to both suspended and sedimentary OM by applying a dual carbon isotope ($\delta^{13}C$ and F_m), three-source mixing model previously utilized for DIC (supplementary material A-4). The $\delta^{13}C$ and F_m values of OM sources in R_{pp}, subsoil and deep soil are shown in Table 2. We have found no reported study of the OM composition of bedrock outcropping or beneath the weathered soil in the Pearl River basin. We therefore use the data for most-proximal rock samples collected within the Upper Permian Xuanwei and Lower Triassic Kayitou Formations in western Guizhou and eastern Yunnan of the middle Pearl River basin (Cui et al., 2017), as the petrogenic OC endmember. The geological map of the Pearl River (Fig. 1c) illustrates that the Permian/Triassic bedrocks dominate the upper and middle Pearl River basin, where significant amounts of sediment is exported to the river. Hence, the OM composition of these bedrocks is considered as a representative petrogenic OC endmember. The average $\delta^{13}C$ of OM in these bedrocks was estimated at $-24.8 \pm 1.8‰$ (Cui et al., 2017). In general, the petrogenic OC is characterized by low OC content and absence of ^{14}C (F_m: 0). Given the relatively large uncertainties of each OM source (Fig. 10), a Bayesian based MixSIAR model was adopted to estimate each fraction more accurately (Moore and Semmens, 2008). For the OM composition of the soil endmember in the mixing model, subsoil was used for SPM, while deep soil was adopted for deposited sediment. The model results are shown in Fig. 10 and Tables 3 and A3.

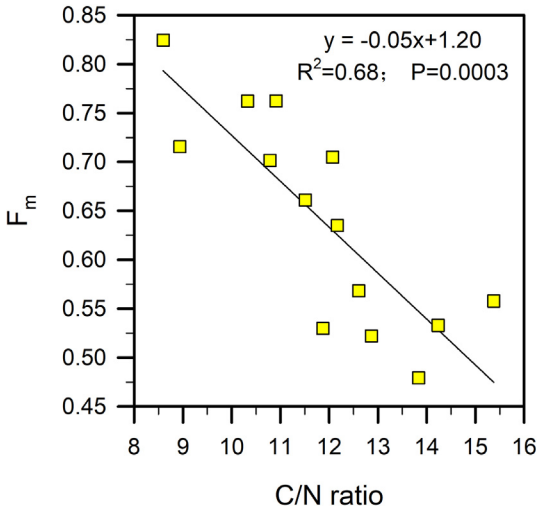

Fig. 9. Radiocarbon concentration expressed as F_m versus C/N ratio in the West river sediments.

The model results reveal that both suspended and sedimentary OM are dominated by the soil-derived OM, but exhibit different contributions from R_{pp} and petrogenic OC (Fig. 10b; Table 3). Given ~90% of the annual suspended flux is supplied during the wet season, we calculate annually averaged contributions from soil, R_{pp}, and petrogenic OC to SPM are 72 ± 1.6, 12 ± 0.3, and $16 \pm 1.5\%$, respectively. Likewise, the averaged contributions from these sources to sediment are 92 ± 7, 0.2 ± 0.0, and $7 \pm 4\%$, respectively. The fractions of R_{pp} and petrogenic OC contributing to SPM were higher in the dry season ($17 \pm 2\%$ and $20 \pm 3\%$, respectively; Table 3) than in the wet season ($11 \pm 0\%$ and $15 \pm 3\%$). Correspondingly, the contributions from soils (OC_{soil}) to SPM remain relatively stable for both wet and dry season samples ($1.20 \pm 0.50\%$ vs. $1.05 \pm 0.18\%$; Fig. 10b), while the OC content of the R_{pp} (OC_{Rpp}) increased from wet ($0.16 \pm 0.03\%$) to dry season SPM ($0.32 \pm 0.15\%$). During the dry season, the clear, sunlit water and more stable substrate would significantly enhance the growth of R_{pp} in the water column.

The contents of OC_{soil}, OC_{Rpp} and OC_{petro} in year-averaged SPM are higher than those in sediments (1.07 ± 0.19 vs. $0.71 \pm 0.36\%$, 0.18 ± 0.03 vs. $0.002 \pm 0.001\%$ and 0.24 ± 0.06 vs. $0.05 \pm 0.06\%$). These differences can be attributed to either different grain sizes or to the OC degradation during settling and intermediate storage. Grain-size data is not available for the SPM (Wei et al., 2010; Sun et al., 2015) and thus the effect of grain size between SPM and sediment cannot be assessed and can be taken into consideration for future studies. On the other hand, the Dinghushan soil OC content decreased with depth irrespective of changes in grain size (Fig. A11; Chen et al., 2002a), indicating that the degradation process far outweighs the grain size in controlling the soil OC content in the Pearl River catchment. Therefore, composition of suspended and sedimentary OM must also be primarily controlled by OC degradation. Consistently, during settling and storage, almost all OM sourced by R_{pp} is degraded and only ~$23 \pm 31\%$ of OC_{petro} and $67 \pm 22\%$ of OC_{soil} in SPM is preserved in sediments. If this is the case, petrogenic OC

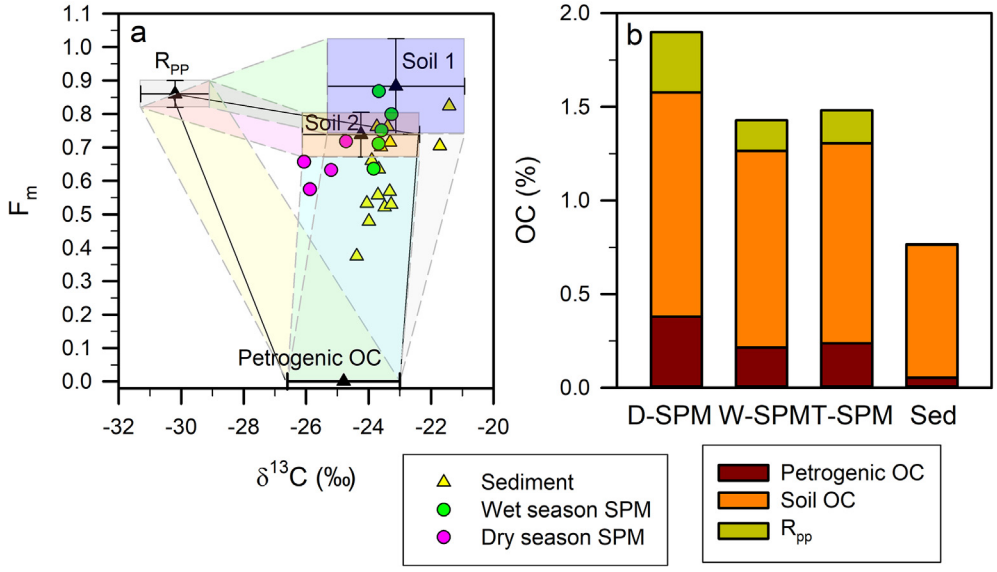

Fig. 10. (a) $\delta^{13}C$ and F_m for suspended particulate matter (SPM) and sediment with their potential sources, including riverine primary productivity (R_{PP}), subsoil (Soil 1), deep soil (Soil 2) and petrogenic OC, and (b) the amount of OC derived from three different sources, R_{PP}, soil and petrogenic OC, in the dry season SPM (D-SPM), wet season SPM (W-SPM), and total yearly SPM (T-SPM), and sediment (Sed). The isotopic compositions of each source in Panel a are represented by mean values with 1-standard deviation.

Table 3
Model results of proportional fractions of OM sources, including riverine primary production (R_{pp}), soil, and petrogenic OC, for the suspended particulate matter (SPM) and sediment in the Pearl River.

	Soil % Mean ± SD (Range)	R_{pp} % Mean ± SD (Range)	Bedrock % Mean ± SD (Range)
Dry season SPM	63 ± 5 (58–69)	17 ± 2 (7–24)	20 ± 3 (17–24)
Wet season SPM	73 ± 3 (69–77)	11 ± 0 (11–12)	15 ± 3 (12–19)
*Annual SPM	72 ± 1.6	12 ± 0.3	16 ± 1.5
Sediment	92 ± 4 (80–97)	0.2 ± 0.0 (0.1–0.3)	7 ± 4 (3–20)

* This is the yearly SPM calculated based on 90% of suspended load from the wet season.

is apparently degraded more extensively than the soil OM fraction. The slower degradation of the latter may reflect its physicochemical protection within mineral lattices that develop during the weathering/soil formation processes (Kennedy et al., 2014). In contrast, petrogenic OC may exist in various forms including discrete particles from a few to several tens of micrometer size, inclusions within quartz, calcite and metamorphic minerals, and aggregates with minerals, mostly micas and highly ordered polycrystalline or pristine graphite (Galy et al., 2008; Blattmann et al., 2018). Partial oxidation of petrogenic OC in the Pearl River may be related to the oxidation of less graphitic OC as a result of enhanced oxygen exposure, dissolution, and biological assimilation processes (Bouchez et al., 2014; Petsch, 2014). In addition, the presence (and degradation) of a small fraction of ancient OC originating from petroleum and pyrogenic black carbon cannot be excluded. Follow-up studies using specific anthropogenic indicators, such as polycyclic aromatic hydrocarbons (PAHs), are needed to elucidate the influence of human activity on the Pearl River OM pool.

The particulate OC flux from the West River in 2005 was estimated at 0.43 Tg (Sun et al., 2007), accounting for 0.2% of the global particulate OC flux (Schlünz and Schneider, 2000). This represents a comprehensive estimation given that it is based on a high sampling frequency including the flood events. Given the basin area of 0.35×10^6 km^2, the corresponding particulate OC yield (1.23 t km^{-2} yr^{-1}) is slightly lower than the global particulate OC yield (1.86 t km^{-2} yr^{-1}) estimated by Galy et al. (2015). Our estimates reveal that this particulate OC consists of 72 ± 1.6% soil OC, 12 ± 0.3% recently-produced R_{pp}, and 16 ± 1.5% petrogenic OC, corresponding to annual fluxes of 0.31 ± 0.01 Tg OC_{soil}, 0.05 ± 0.00 Tg OC_{Rpp} and 0.07 ± 0.01 Tg OC_{petro}. As the R_{pp} is easily degraded, ~0.38 ± 0.02 Tg OC yr^{-1} is likely surviving degradation during transport to the Pearl River estuary and further to the northern South China Sea. This estimated particulate OC flux exported to the ocean from the Pearl River (0.38 ± 0.02 Tg yr^{-1}) would be equivalent to half of the CO_2 flux consumed by silicate weathering in the West River system (0.77 Tg yr^{-1}; Gao et al., 2009). While oxidation of relatively labile soil- and R_{pp} -sourced OM contributes CO_2 to the atmosphere, the export and burial of refractory soil- and ancient rock-sourced OM thus represent a significant CO_2 sink. Recycling and re-burial of

ancient rock-sourced OM exert no influence on atmospheric CO_2 (Galy et al., 2008), while oxidation of this material serves as a source of CO_2 to the atmosphere. Collectively, these processes are relevant for the short- and long-term global carbon cycle.

4.6. Longitudinal evolution of suspended and sedimentary OM

The estimates described above are based on an average values and are discussed accordingly, but there are also longitudinal gradients of suspended and sedimentary OM content and composition. While these gradients do not always follow consistent patterns, in general there is a downstream decreasing trend in $\delta^{13}C$ values of suspended (Fig. 11a; Sun et al., 2015) and sedimentary OM (Fig. 3a). The F_m values of the dry season suspended OM increase downstream (Fig. 11b), but slightly decrease for the wet season suspended OM (Fig. 11b) and sedimentary OM (Fig. 3b). There may be various explanations for these gradients, including changes in vegetation (e.g. C3 vs. C4 plants), formation and degradation of R_{pp}, degradation of soil OM, and the contribution of petrogenic OC (e.g. Tamooh et al., 2012; Leithold et al., 2016).

4.6.1. Suspended OM

A downstream trend of decreasing $\delta^{13}C$ values from −23.5‰ to −26.2‰ is evident in the dry season suspended OM, while this trend is not apparent for the wet season (Fig. 11a; Sun et al., 2015). Dry season SPM comprises 63 ± 5, 17 ± 2 and $20 \pm 3\%$ of soil, R_{pp}, and petrogenic OC, respectively (Section 4.5). Oxidative loss of certain OM components can be excluded as the OC contents in dry season SPM increase downstream. Given similar $\delta^{13}C$ values for soil and petrogenic OC (-23.2 ± 2.2 vs. -24.8 ± 1.8‰), differential mixing of these two components would not change suspended OM $\delta^{13}C$ values significantly, but would alter F_m values. In contrast, increasing OM contribution from R_{pp} ($\delta^{13}C$: −30.0‰ and F_m: 0.86) would result in a decrease in $\delta^{13}C$ values and an increase in F_m values, while the increasing OM contribution from soil would increase both $\delta^{13}C$ and F_m, as the $\delta^{13}C$ and F_m values in soil OM are higher than the upstream suspended OM (−23.3 vs. −23.5‰ and 0.87 vs. 0.65). We therefore suggest that the R_{pp} inputs are responsible for the longitudinal changes observed in the OM composition of dry season SPM. This is consistent with the increasing F_m downstream in 2015 (Fig. 11b; Liu et al., 2017). For the wet season suspended OM, the slightly decrease in $\delta^{13}C$ values downstream can also be attributed to increasing input of R_{pp}, however, the latter is of lesser importance during the wet season compared to the dry season.

The basin-wide variation of soil OM composition largely depends on the distribution of vegetation types, C3 and C4 plants, serving as another potential explanation for decreasing $\delta^{13}C$ values downstream. Sun et al. (1999) reported that the agricultural land (C3 and C4 plants) and conifer-forests (C3 plants) are dominant in the lower drainage basin, while grasses (mostly C4 plants) dominate in the upper drainage basin. This vegetation pattern would produce higher $\delta^{13}C$ values for soil OM in the upper reaches compared to the lower reaches of the river basin, consistent with $\delta^{13}C$ values (−24.8 to −18.8‰) reported for SPM in the Yujiang, a tributary in the West River upstream (Fig. 1a; Liu et al., 2017). However, attributing this trend in a $\delta^{13}C$ values solely to spatial variation in C3/C4 vegetation is inconsistent with the relatively low and downstream decreasing trend in F_m values. Instead, the positive relationship between F_m values of suspended OM and DIC (supplementary material A-4) supports the argument that increasing OM contribution from R_{pp} is the primary influence on the composition of suspended OM downstream. Hence, we infer that geochemical differences of suspended OM observed along the river are largely due to variations in R_{pp}, with subordinate influence from other processes such as OM degradation and fractional change in C3/C4 plants.

4.6.2. Sedimentary OM

When compared to the suspended OM, sedimentary OM exhibits minor downstream gradients of decreasing TOC, F_m, and $\delta^{13}C$, while C/N ratios increase (Figs. 2 and 3).

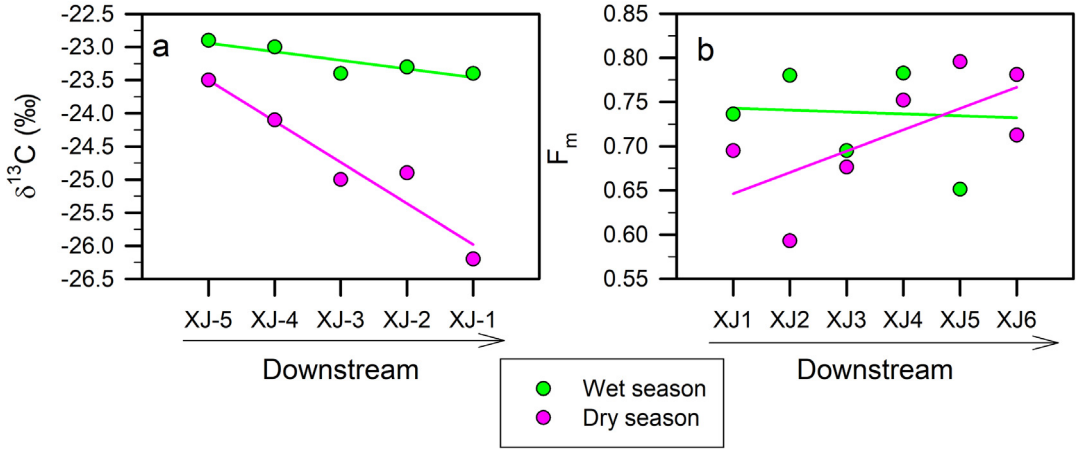

Fig. 11. Downstream variation of (a) $\delta^{13}C$ and (b) F_m for the wet and dry season suspended OM along the West River. As there is no F_m data available for 2004 and 2005 (Sun et al., 2015), F_m data of suspended OM from 2014 and 2015 are plotted (Liu et al., 2017).

The weak trend in F_m suggests that in-river degradation may play a role. The mineral surface area-normalized TOC content of sediments, i.e. the OC/SA ratio or OC loading, can be used to evaluate the influence OM degradation by accounting for grain sizes variations resulting from physical sorting of particles during transport (Keil et al., 1994, 1997; Blair and Aller, 2012). OC/SA ratios between 0.4 and 1.0 mg/m^2 represent typical OC loadings for riverine SPM (Blair and Aller, 2012) that reflect the carrying capacity of mineral for OC (Mayer, 1994a, 1994b). In the West River, most sediments display OC loadings below 0.4 mg/m^2, with OC loadings further decreasing towards downstream (Fig. 4d). Similar low and longitudinally decreasing OC loadings have also been found in other passive margin rivers, such as Danube (Freymond et al., 2018), Godavari (Usman et al., 2018), Tana (Tamooh et al., 2012) and Ganges (Galy et al., 2008). This suggests that OM degradation in sediments during resuspension and fluvial transport is an important process, with degradation due to biogeochemical processes and particle sorting resulting from physical processes operating simultaneously. Collectively, these processes/changes determine the composition of OM in river sediments. A simple conservative mixing of source components thus cannot fully explain the observed OM composition of SPM and sediments in large rivers. Consideration of dynamic, age-related degradation processes of OM components along the watershed-river corridor is essential to fully understand the fate of OM in global river systems.

5. CONCLUSIONS

Elemental and isotopic data (C/N ratio, $\delta^{13}C$ and F_m) of sedimentary OM were determined and combined with literature data on SPM and soil profiles in the Pearl River watershed in order to provide a basin-wide picture on the origin and processing of OM in this large subtropical fluvial system. The OM sources for SPM and sediment are derived from soil, in-situ produced riverine OM (R_{pp}) and petrogenic OC with negligible direct input from terrestrial vegetation. SPM ($72 \pm 1.6\%$) and sediment ($92 \pm 4\%$) are dominated by soil-derived OM, with different soil OM components varying in reactivity from readily degradable OM from top soil (degradation rate of 0.36 yr^{-1}), moderately degradable OM (0.0051–0.0071 yr^{-1}), to highly refractory OM derived from deep soils (0.0002–0.0003 yr^{-1}). During erosion and transport, the most labile, top soil-derived OM is degraded and contributing to riverine DIC. In contrast, the more refractory OM in deeper mineral soils comprises the main (residual) component of SPM. During deposition and storage, moderately labile soil OM is further degraded, leaving the most refractory OM fraction to be predominate in the sediments.

The R_{pp} -derived fraction in suspended OM is higher during the dry than the wet season ($17 \pm 2\%$ vs. $11 \pm 0\%$). This reactive R_{pp} OM is mostly degraded during settling and deposition, leaving only a small proportion ($0.2 \pm 0.2\%$) of its initial amount in the sediments. Petrogenic OC mobilized from ancient bedrock contributes $15 \pm 3\%$ to the wet season SPM, and $20 \pm 3\%$ for the dry season SPM and $7 \pm 4\%$ to the sediment. By comparing the amounts of three OC sources in SPM and sediment, we estimate that 30% of soil OM, 99% of the R_{pp}, and 75% of petrogenic OC are degraded during settling and deposition processes. More soils are mobilized and exposed to the oxygen during the wet season or flood event. The resulting enhanced degradation of soil OM will result in an increased fraction of soil-derived CO_2 in riverine wet season DIC compare to dry season DIC ($31 \pm 2\%$ vs. $39 \pm 1\%$). The longitudinal evolution of the DIC isotopic composition along the river is mainly controlled by the contribution from soil OM degradation. The along-river evolution of suspended OM composition is mainly controlled by both variable contributions of R_{pp} and degradation processes, whereas the longitudinal evolution of sedimentary OM is dominated by degradation processes. This study provides a first-order synthesis for OM sources, dynamics and related processes for the Pearl River. More comprehensive understanding of OC cycling and its longitudinal evolution with this and other fluvial systems would require simultaneous measurement of a broader suite of parameters in suspended and deposited sediments as well as dissolved load from headwater to river outlet and include in-depth investigation of organic components in order to better differentiate different OM sources and to assess their degradation and preservation pathways.

ACKNOWLEDGMENTS

We thank Christophe Colin and Zhong Chen for assistance during fieldwork sampling, Yanli Li and Daniel Montluçon for technical and laboratory assistance and all members of Ion Beam Physics Laboratory at ETH for ^{14}C measurement. This work was supported by the National Natural Sciences Foundation of China (Nos. 91528304 and 41530964) and by the Swiss National Science Foundation (No. 200020_163162). BL thanks the China Scholarship Council (201706260239) for the support during her stay at ETH Zürich (Switzerland). We are grateful to Jeffrey G. Catalano and Sarah Feakins for handling the manuscript and three anonymous referees for their thorough and insightful reviews.

APPENDIX A. SUPPLEMENTARY MATERIAL

Supplementary data to this article can be found online at https://doi.org/10.1016/j.gca.2019.06.018.

REFERENCES

Alin Simone R., Aalto Rol, Goni Miguel A., Richey Jeffrey E. and Dietrich William E. (2008) Biogeochemical characterization of carbon sources in the Strickland and Fly rivers, Papua New Guinea. *J. Geophys. Res.* **113**(F1). https://doi.org/10.1029/2006JF000625.

Aufdenkampe A. K., Mayorga E., Raymond P. A., Melack J. M., Doney S. C., Alin S. R., Aalto R. E. and Yoo K. (2011) Riverine coupling of biogeochemical cycles between land, oceans, and atmosphere. *Front. Ecol. Environ* **9**, 53–60.

Bauer J. E., Cai W. J., Raymond P. A., Bianchi T. S., Hopkinson C. S. and Regnier P. A. (2013) The changing carbon cycle of the coastal ocean. *Nature* **504**, 61–70.

Berner R. A. (1982) Burial of organic carbon and pyrite sulfur in the modern ocean: its geochemical and environmental significance. *Am. J. Sci.* **282**, 451–473.

Berner R. A. (1989) Biogeochemical cycles of carbon and sulfur and their effect on atmospheric oxygen over Phanerozoic time. *Glob. Planet. Change* **1**, 97–122.

Blair N. E. and Aller R. C. (2012) The fate of terrestrial organic carbon in the marine environment. *Annu. Rev. Mar. Sci.* **4**, 401–423.

Blair N. E., Leithold E. L. and Aller R. C. (2004) From bedrock to burial: the evolution of particulate organic carbon across coupled watershed-continental margin systems. *Mar. Chem.* **92**, 141–156.

Blair N. E., Leithold E. L., Ford S. T., Peeler K. A., Holmes J. C. and Perkey D. W. (2003) The persistence of memory: the fate of ancient sedimentary organic carbon in a modern sedimentary system. *Geochim. Cosmochim. Acta* **67**, 63–73.

Blattmann T. M., Letsch D. and Eglinton T. I. (2018) On the geological and scientific legacy of petrogenic organic carbon. *Am. J. Sci.* **318**, 861–881.

Blattmann T. M., Wessels M., McIntyre C. P. and Eglinton T. I. (2019) Petrogenic organic carbon retention in terrestrial basins: a case study from perialpine Lake Constance. *Chem. Geol.* **503**, 52–60.

Bouchez J., Beyssac O., Galy V., Gaillardet J., France-Lanord C., Maurice L. and Moreira-Turcq P. (2010) Oxidation of petrogenic organic carbon in the Amazon floodplain as a source of atmospheric CO_2. *Geology* **38**, 255–258.

Bouchez J., Galy V., Hilton R. G., Gaillardet J., Moreira-Turcq P., Pérez M. A., France-Lanord C. and Maurice L. (2014) Source, transport and fluxes of Amazon River particulate organic carbon: insights from river sediment depth-profiles. *Geochim. Cosmochim. Acta* **133**, 280–298.

Broecker W. S. and Olson E. A. (1961) Lamont radiocarbon measurements VIII. *Radiocarbon* **3**, 176–204.

Brunauer S., Emmett P. H. and Teller E. (1938) Adsorption of gases in multimolecular layers. *J. Am. Chem. Soc.* **60**, 3095–3019.

Burdige David J. (2005) Burial of terrestrial organic matter in marine sediments: a re-assessment. *Global Biogeochem. Cycles* **19**(4), GB4011. https://doi.org/10.1029/2004GB002368.

Cartapanis O., Bianchi D., Jaccard S. L. and Galbraith E. D. (2016) Global pulses of organic carbon burial in deep-sea sediments during glacial maxima. *Nat. Commun.* **7**, 10796. https://doi.org/10.1038/ncomms10796.

Chen Q. Q., Shen C. D., Peng S. L., Sun Y. M., Yi W. X., Li Z. A. and Jiang M. T. (2002a) Soil organic matter turnover in the subtropical mountainous region of South China. *Soil Sci.* **167**, 401–415.

Chen Q. Q., Sun Y. M., Shen C. D., Peng S. L., Yi W. X., Li Z. A. and Jiang M. T. (2002b) Organic matter turnover rates and CO_2 flux from organic matter decomposition of mountain soil profiles in the subtropical area, south China. *Catena* **49**, 217–229.

Clark K. E., Hilton R. G., West A. J., Malhi Y., Gröcke D. R., Bryant C. L., Ascough P. L., Robles Caceres A. and New M. (2013) New views on "old" carbon in the Amazon River: insight from the source of organic carbon eroded from the Peruvian Andes. *Geochem. Geophys. Geosystems* **14**, 1644–1659.

Cole J. J., Prairie Y. T., Caraco N. F., McDowell W. H., Tranvik L. J., Striegl R. G., Duarte C. M., Kortelainen P., Downing J. A., Middelburg J. J. and Melarck J. (2007) Plumbing the global carbon cycle: integrating inland waters into the terrestrial carbon budget. *Ecosystems* **10**, 171–184.

Cui Y., Bercovici A., Yu J., Kump L. R., Freeman K. H., Su S. and Vajda V. (2017) Carbon cycle perturbation expressed in terrestrial Permian-Triassic boundary sections in South China. *Glob. Planet. Change* **148**, 272–285.

Doetterl S., Berhe A. A., Nadeu E., Wang Z., Sommer M. and Fiener P. (2016) Erosion, deposition and soil carbon: a review of process-level controls, experimental tools and models to address C cycling in dynamic landscapes. *Earth-Sci. Rev.* **154**, 102–122.

Ehleringer J. R., Lin Z. F., Field C. B., Sun G. C. and Kuo C. Y. (1987) Leaf carbon isotope ratios of plants from a subtropical monsoon forest. *Oecol. (Berlin)* **72**, 109–114.

Fang Y., Yoh M., Koba K., Zhu W., Takebayashi Y. U., Xiao Y., Lei C., Mo J., Zhang W. and Lu X. (2011) Nitrogen deposition and forest nitrogen cycling along an urban–rural transect in southern China. *Glob. Change Biol.* **17**, 872–885.

Freymond C. V., Kündig N., Stark C., Peterse F., Buggle B., Lupker M., Plötze M., Blattmann T. M., Filip F., Giosan L. and Eglinton T. I. (2018) Evolution of biomolecular loadings along a major river system. *Geochim. Cosmochim. Acta* **223**, 389–404.

Fry B. and Sherr E. B. (1989) $\delta^{13}C$ measurements as indicators of carbon flow in marine and freshwater ecosystems. In *Stable Isotopes in Ecological Research*. Springer, New York, NY, pp. 196–229.

Galy V. and Eglinton T. I. (2011) Protracted storage of biospheric carbon in the Ganges-Brahmaputra basin. *Nature Geosci.* **4**, 843–847.

Galy V., Beyssac O., France-Lanord C. and Eglinton T. I. (2008) Recycling of graphite during Himalayan erosion: a geological stabilization of carbon in the crust. *Science* **322**, 943–945.

Galy V., France-Lanord C., Beyssac O., Faure P., Kudrass H. and Palhol F. (2007) Efficient organic carbon burial in the Bengal fan sustained by the Himalayan erosional system. *Nature* **450**, 407–410.

Galy V., Peucker-Ehrenbrink B. and Eglinton T. (2015) Global carbon export from the terrestrial biosphere controlled by erosion. *Nature* **521**, 204–207.

Gao Q., Tao Z., Huang X., Nan L., Yu K. and Wang Z. (2009) Chemical weathering and CO2 consumption in the Xijiang River basin, South China. *Geomorphology* **106**, 324–332.

Goñi M. A., Moore E., Kurtz A. K., Portier E., Alleau Y. and Merrell D. (2014) Organic matter compositions and loadings in soils and sediments along the Fly River, Papua New Guinea. *Geochim. Comochim. Acta* **140**, 275–296.

Han G., Li F. and Tang Y. (2015) Variations in soil organic carbon contents and isotopic compositions under different land uses in a typical karst area in Southwest China. *Geochem. J.* **49**, 63–71.

He B., Dai M., Huang W., Liu Q., Chen H. and Xu L. (2010) Sources and accumulation of organic carbon in the Pearl River estuary surface sediment as indicated by elemental, stable carbon isotopic, and carbohydrate compositions. *Biogeosciences* **7**, 3343–3362.

Hedges J. I. and Oades J. M. (1997) Comparative organic geochemistries of soils and marine sediments. *Org. Geochem.* **27**, 319–361.

Hedges J. I., Keil R. G. and Benner R. (1997) What happens to terrestrial organic matter in the ocean? *Org. Geochem.* **27**, 195–212.

Hemingway J. D., Hilton R. G., Hovius N., Eglinton T. I., Haghipour N., Wacker L., Chen M. and Galy V. V. (2018) Microbial oxidation of lithospheric organic carbon in rapidly eroding tropical mountain soils. *Science* **360**, 209–212.

Hilton R. G., Galy A., Hovius N., Horng M. J. and Chen H. (2010) The isotopic composition of particulate organic carbon in mountain rivers of Taiwan. *Geochim. Cosmochim. Acta* **74**, 3164–3181.

Huang J. X. and Lin T. S. (1983) The characteristics of karst groundwater in Zhujiang watershed (research report). *Pearl River* **6**, 14–17 (in Chinese).

Huguet C., de Lange G. J., Gustafsson Ö., Middelburg J. J., Damsté J. S. S. and Schouten S. (2008) Selective preservation of soil organic matter in oxidized marine sediments (Madeira Abyssal Plain). *Geochim. Cosmochim. Acta* **72**, 6061–6068.

Janssen B. H. (1984) A simple method for calculating decomposition and accumulation of 'young' soil organic matter. *Plant Soil* **76**, 297–304.

Kandasamy S. and Nagender Nath Nath B. (2016) Perspectives on the terrestrial organic matter transport and burial along the land-deep sea continuum: Caveats in our understanding of biogeochemical processes and future needs. *Front. Mar. Sci.* **3**. https://doi.org/10.3389/fmars.2016.00259.

Keil R. G., Mayer L. M., Quay P. D., Richey J. E. and Hedges J. I. (1997) Loss of organic matter from riverine particles in deltas. *Geochim. Cosmochim. Acta* **61**, 1507–1511.

Keil R. G., Montluçon D. B., Prahl F. G. and Hedges J. I. (1994) Sorptive preservation of labile organic matter in marine sediments. *Nature* **370**, 549–552.

Kennedy M. J., Löhr S. C., Fraser S. A. and Baruch E. T. (2014) Direct evidence for organic carbon preservation as clay-organic nanocomposites in a Devonian black shale; from deposition to diagenesis. *Earth Planet. Sci. Lett.* **388**, 59–70.

Komada T., Anderson M. R. and Doreier C. L. (2008) Carbonate removal from coastal sediments for the determination of organic carbon and its isotopic signatures, $\delta^{13}C$ and $\Delta^{14}C$: comparison of fumigation and direct acidification by hydrochloric acid. *Limnol. Oceanogr.: Methods* **6**, 254–262.

Leithold E. L., Blair N. E. and Wegmann K. W. (2016) Source-to-sink sedimentary systems and global carbon burial: a river runs through it. *Earth-Sci. Rev.* **153**, 30–42.

Li G.R. (2009) Cascade damming of the river and phytoplankton evolution recorded by carbon isotopic composition: a case study on the Maotiaohe River. Master Degree Thesis. Guizhou Normal University (in Chinese).

Li G., Wang X. T., Yang Z., Mao C., West A. J. and Ji J. (2014) Dam-triggered organic carbon sequestration makes the Changjing (Yangtze) river basin (China) a significant carbon sink. *J. Geophys. Res. Biogeosci.* **120**, 39–53.

Li X. X., Zhang Z. R., Wade T. L., Knap A. H. and Zhang C. L. (2017) Sources and compositional distribution of organic carbon in surface sediments from the lower Pearl River to the coastal South China Sea. *J. Geophys. Res. Biogeosci.* **122**, 2104–2117.

Liu Z., Colin C., Huang W., Le K. P., Tong S., Chen Z. and Trentesaux A. (2007) Climatic and tectonic controls on weathering in South China and the Indochina Peninsula: clay mineralogical and geochemical investigations from the Pearl, Red, and Mekong drainage basins. *Geochem. Geophys. Geosystems* **8**, Q05005. https://doi.org/10.1029/2006GC001490.

Liu Z., Zhao Y., Colin C., Stattegger K., Wiesner M. G., Huh C.-A., Zhang Y., Li X., Sompongchaiyakul P., You C.-F., Huang C.-Y., Liu J. T., Siringan F. P., Le K. P., Sathiamurthy E., Hantoro W. S., Liu J., Tuo S., Zhou S., He Z., Wang Y., Bunsomboonsakul S. and Li Y. (2016) Source-to-sink processes of fluvial sediments in the South China Sea. *Earth-Sci. Rev.* **153**, 238–273.

Liu Z. H., Zhao M., Sun H. L., Yang R., Chen B., Yang M. X., Zeng Q. R. and Zeng H. T. (2017) "Old" carbon entering the South China Sea from the carbonate-rich Pearl River Basin: Coupled action of carbonate weathering and aquatic photosynthesis. *Appl. Geochem.* **78**, 96–104.

Ludwig W. (2001) Carbon cycle: the age of river carbon. *Nature* **409**, 466–467.

Luk S. H., Yao Q. Y., Gao J. Q., Zhang J. Q., He Y. G. and Huang S. M. (1997) Environmental analysis of soil erosion in Guangdong Province: a Deqing case study. *Catena* **29**, 97–113.

Marwick T. R., Tamooh F., Teodoru C. R., Borges A. V., Darchambeau F. and Bouillon S. (2015) The age of river-transported carbon: a global perspective. *Glob. Biogeohem. Cycles* **29**, 122–137.

Mayer L. M. (1994a) Relationship between mineral surfaces and organic carbon concentrations in soils and sediments. *Chem. Geol.* **114**, 347–363.

Mayer L. M. (1994b) Surface area control of organic carbon accumulation in continental shelf sediments. *Geochim. Cosmochim. Acta* **58**, 1271–1284.

Meyers P. A. (1994) Preservation of elemental and isotopic source identification of sedimentary organic matter. *Chem. Geol.* **114**, 289–302.

Middelburg J. J. (1989) A simple rate model for organic matter decomposition in marine sediments. *Geochim. Cosmochim. Acta* **53**, 1577–1581.

Milliman J. D. and Farnsworth K. L. (2011) Runoff, erosion, and delivery to the coastal ocean. *River Discharge Coast. Ocean: A Global Synth.*, 13–61.

Moore J. W. and Semmens B. X. (2008) Incorporating uncertainty and prior information into stable isotope mixing models. *Ecol. Let.* **11**, 470–480.

Pearl River Water Resources Committee (PRWRC) (1991) The Zhujiang Archive, vol. 1. Guangdong Science and Technology Press, Guangzhou, in Chinese.

Petsch S. T. (2014) Weathering of organic carbon. In *Treatise on Geochemistry* (eds. H. D. Holland and K. K. Turekian), second ed, pp. 217–218. The Zhujiang Archive. https://doi.org/10.1016/B978-0-08-095975-7.01013-5.

Prahl F. G., Cowie G. L., De Lange G. J. and Sparrow M. A. (2003) Selective organic matter preservation in "burn-down" turbidites on the Madeira Abyssal Plain. *Paleoceanography* **18**. https://doi.org/10.1029/2002PA000853.

Rau G. H. (1994) Variations in sedimentary organic $\delta^{13}C$ as a proxy for past changes in ocean and atmospheric CO_2 concentrations. In *Carbon cycling in the glacial ocean: constraints on the ocean's role in global change*. Springer, Berlin, Heidelberg, pp. 307–321.

Raymond P. A., Bauer J. E., Caraco N. F., Cole J. J., Longworth B. and Petsch S. T. (2004) Controls on the variability of organic matter and dissolved inorganic carbon ages in northeast US rivers. *Mar. Chem.* **92**, 353–366.

Sarmiento J. L. and Gruber N. (2002) Sinks for anthropogenic carbon. *Phys. Today* **55**, 30–36.

Schlünz B. and Schneider R. R. (2000) Transport of terrestrial organic carbon to the oceans by rivers: re-estimating flux- and burial rates. *Int. J. Earth Sci.* **88**, 599–606.

Shen C. D., Sun Y. M., Yi W. X., Peng S. L. and Li Z. A. (2001) Carbon isotope tracers for the restoration of degenerated forest ecosystem. *Quat. Sci.* **21**, 452–460, in Chinese.

Shen C. D., Yi W. X., Sun Y. M., Xing C. P., Yang Y., Peng S. L. and Li Z. A. (2000) ^{14}C apparent ages and soil in Dinghushan natural reserve. *Quat. Sci.* **20**, 335–344, in Chinese.

Shen Y. T., Lu G. H., Hu J. D. and Wang X. J. (2012) ^{13}C distribution characteristics in soil profiles with the impacts of short-term trees, shrubs and grass replacement. *Prog. Geogr.* **31**, 1460–1466, in Chinese.

Siegenthaler U. and Sarmiento J. L. (1993) Atmospheric carbon dioxide and the ocean. *Nature* **365**, 119–125.

Stuiver M. and Polach H. A. (1977) Discussion: reporting of ^{14}C data. *Radiocarbon* **19**, 355–363.

Sun H., Han J., Zhang S. and Lu X. (2007) The impacts of '05.6'extreme flood event on riverine carbon fluxes in Xijiang River. *Chin. Sci. Bull.* **52**, 805–812.

Sun H. G., Han J. T., Zhang S. R. and Lu X. X. (2015) Carbon isotopic evidence for transformation of DIC to POC in the lower Xijiang River, SE China. *Quat. Int.* **380–381**, 288–296.

Sun X., Li X. and Beug H. J. (1999) Pollen distribution in hemipelagic surface sediments of the South China Sea and its relation to modern vegetation distribution. *Mar. Geol.* **156**, 211–226.

Synal H. A., Stocker M. and Suter M. (2007) MICADAS: a new compact radiocarbon AMS system. *Nucl. Instr. Methods Phys. Res. Sect. B: Beam Interact. Mater. Atoms* **259**, 7–13.

Syvitski J. P., Vörösmarty C. J., Kettner A. J. and Green P. (2005) Impact of humans on the flux of terrestrial sediment to the global coastal ocean. *Science* **308**, 376–380.

Tamooh F., Van den Meersche K., Meysman E., Marwick T. R., Borges A. V., Merckx R., Dehairs F., Schmidt S., Nyunja J. and Bouillon S. (2012) Distribution and origin of suspended matter and organic carbon pools in the Tana River Basin, Kenya. *Biogeosciences* **9**, 2905–2920.

Tao S., Eglinton T. I., Zhang L., Yi Z., Montluçon D. B., McIntyre C., Yu M. and Zhao M. (2018) Temporal variability in composition and fluxes of Yellow River particulate organic matter. *Limnol. Oceanogr.* **63**, S119–S141.

Usman M. O., Kirkels F. M. S. A., Zwart H. M., Basu S., Ponton C., Blattmann T. M., Ploetze M., Haghipour N., McIntyre C., Peterse F. and Lupke M. (2018) Reconciling drainage and receiving basin signatures of the Godavari River system. *Biogeosciences* **15**, 3357–3375.

Wacker L., Christl M. and Synal H. A. (2010) Bats: a new tool for AMS data reduction. *Nucl. Instr. Methods Phys. Res. Sect. B: Beam Interact. Mater. Atoms* **268**, 976–979.

Wang X. C., Ma H. Q., Li R. H., Song Z. S. and Wu J. P. (2012) Seasonal fluxes and source variation of organic carbon transported by two major Chinese Rivers: the Yellow River and Changjiang (Yangtze) River. *Glob. Biogeochem. Cycles* **26**, GB2025. https://doi.org/10.1029/2011GB004130.

Wei X. G., Yi W. X., Shen C. D., Yechieli Y., Li N. L., Ding P., Wang N. and Liu K. X. (2010) ^{14}C as a tool for evaluation riverine POC sources and erosion of the Zhujiang (Pearl River) drainage basin, South China. *Nucl. Instrum. Methods Phys. Res. B* **268**, 1094–1097.

Wu C. S., Yang S. L. and Lei Y. P. (2012) Quantifying the anthropogenic and climatic impacts on water discharge and sediment load in the Pearl River (Zhujiang), China (1954–2009). *J. Hydrol.* **452**, 190–204.

Xu Z. and Liu C. Q. (2010) Water geochemistry of the Xijiang basin rivers, South China: chemical weathering and CO_2 consumption. *Appl. Geochem.* **25**, 1603–1614.

Yang M., Liu Z., Sun H., Yang R. and Chen B. (2016) Organic carbon source tracing and DIC fertilization effect in the Pearl River: insights from lipid biomarker and geochemical analysis. *Appl. Geochem.* **73**, 132–141.

Zhu S. and Liu C. (2006) Vertical patterns of stable carbon isotope in soils and particle-size fractions of karst areas, Southwest China. *Environ. Geol.* **50**, 1119–1127.

Associate editor: Sarah J. Feakins